Published December 13, 2010

Molecular architecture of a dynamin adaptor: implications for assembly of mitochondrial fission complexes

Sajjan Koirala, Huyen T. Bui, Heidi L. Schubert, Debra M. Eckert, Christopher P. Hill, Michael S. Kay, and Janet M. Shaw

Department of Biochemistry, University of Utah, Salt Lake City, UT 84112

Recruitment and assembly of some dynamin-related guanosine triphosphatases depends on adaptor proteins restricted to distinct cellular membranes. The yeast Mdv1 adaptor localizes to mitochondria by binding to the membrane protein Fis1. Subsequent Mdv1 binding to the mitochondrial dynamin Dnm1 stimulates Dnm1 assembly into spirals, which encircle and divide the mitochondrial compartment. In this study, we report that dimeric Mdv1 is joined at its center by a 92-Å antiparallel coiled coil (CC). Modeling of the Fis1–Mdv1 complex using available crystal structures suggests that the Mdv1 CC lies parallel to the bilayer with N termini at opposite ends bound to Fis1 and C-terminal β-propeller domains (Dnm1-binding sites) extending into the cytoplasm. A CC length of appropriate length and sequence is necessary for optimal Mdv1 interaction with Fis1 and Dnm1 and is important for proper Dnm1 assembly before membrane scission. Our results provide a framework for understanding how adaptors act as scaffolds to orient and stabilize the assembly of dynamins on membranes.

Introduction

In eukaryotes, mitochondrial fission regulates organelle copy number and mitochondrial function in metabolism, development, and programmed cell death (Chen and Chan, 2005; Okamoto and Shaw, 2005). Fission begins when a dynamin-related GTPase is recruited from the cytoplasm to the outer membrane, where it assembles into large polymers that hydrolyze GTP and sever the mitochondrial compartment. Protein–protein interactions between the GTPase and a membrane-anchored receptor are essential for the recruitment step and are also thought to provide a structural scaffold that promotes GTPase assembly.

The membrane receptor for yeast mitochondrial fission is a complex composed of two proteins, membrane-anchored Fis1 (Mozdy et al., 2000) and its binding partner, Mdv1 (Tieu and Nunnari, 2000; Cerveny et al., 2001; Tieu et al., 2002; Cerveny and Jensen, 2003). Mdv1 functions as an adaptor to bridge the interaction between Fis1 and the cytoplasmic Dnm1 GTPase. Binding of Dnm1 to Mdv1 nucleates the polymerization of Dnm1 dimers into spirals that encircle and constrict the membrane (Bleazard et al., 1999; Ingerman et al., 2005; Bhar et al., 2006; Lackner et al., 2009). Mdv1 coassembles with Dnm1 in these spirals to generate functional fission complexes (Shaw and Nunnari, 2002). Although fission complexes could, in principle, assemble uniformly on the mitochondrial surface, assembly usually occurs at discrete sites on tubular mitochondria in living cells.

The architectural features of the Mdv1–Fis1 receptor required for Dnm1 recruitment and assembly remain unclear. Structural analysis of the Fis1 cytoplasmic domain reveals a single tetratricopeptide repeat (TPR; Suzuki et al., 2005). The N terminus of Mdv1 contains a short, helix-loop-helix motif that surrounds and clamps the surface of the Fis1 TPR domain (Zhang and Chan, 2007). The C terminus of Mdv1, which is required for Dnm1 binding, is predicted to form a multibladed β-propeller. The N- and C-terminal domains are linked by a predicted heptad repeat (HR). Because Mdv1 acts both to recruit Dnm1 and nucleate Dnm1 assembly, defining the structure,

Correspondence to Michael S. Kay: kay@biochem.utah.edu; or Janet M. Shaw: shaw@biochem.utah.edu

Abbreviations used in this paper: CC, coiled coil; CD, circular dichroism; DIC, differential interference contrast; ES, equilibrium sedimentation; HR, heptad repeat; IP, immunoprecipitation; MBP, maltose-binding protein; NTE, N-terminal extension; TPR, tetratricopeptide repeat; WCE, whole cell extract; WT, wild type.

Supplemental Material can be found at:
http://jcb.rupress.org/content/suppl/2010/12/10/jcb.201005046.DC1.html

The Rockefeller University Press $30.00
J. Cell Biol. Vol. 191 No. 6 1127–1139
www.jcb.org/cgi/doi/10.1083/jcb.201005046

Published December 13, 2010

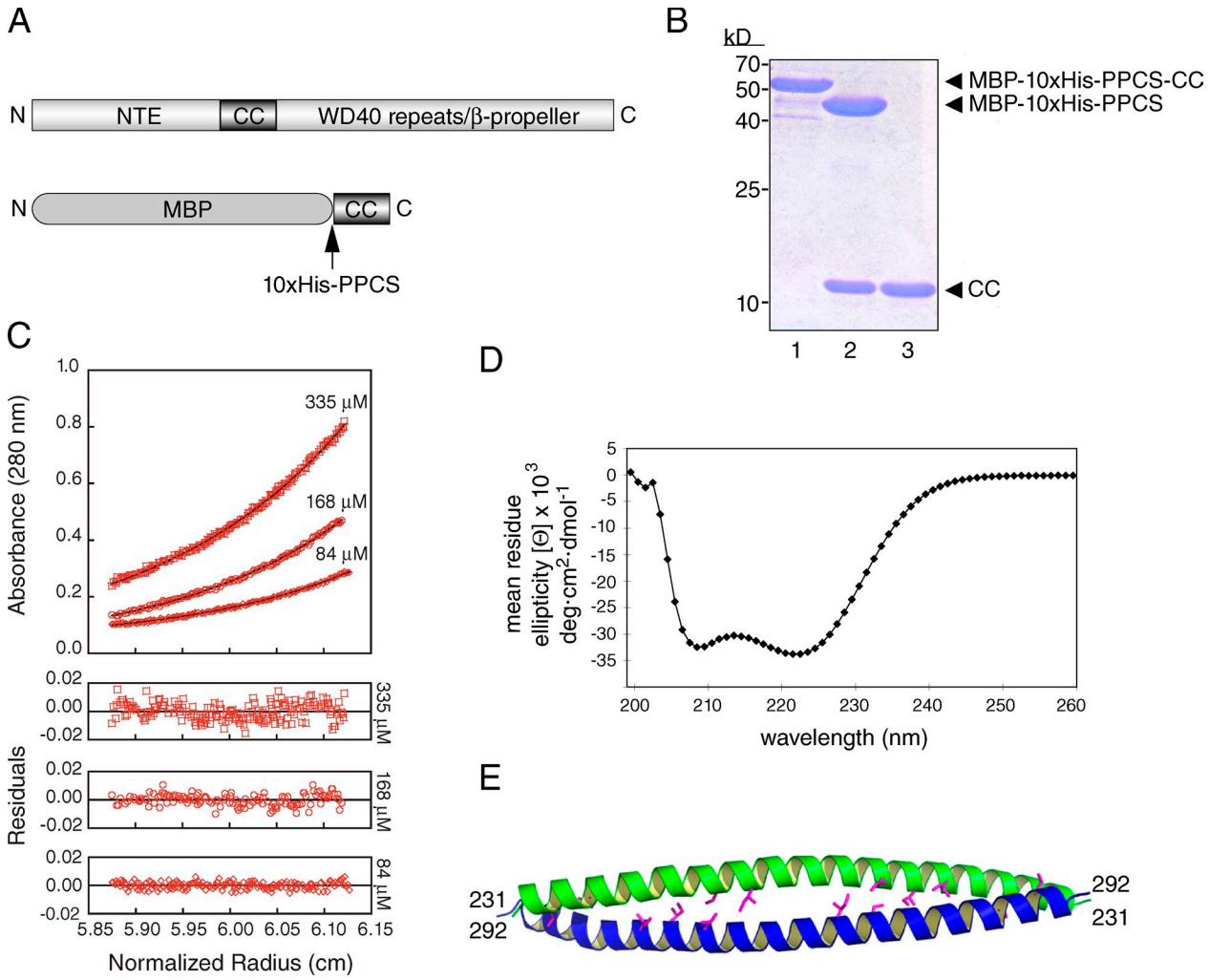

Figure 1. **Mdv1 self-assembles via a dimeric, antiparallel CC.** (A, top) Domain structure of Mdv1, including the NTE, predicted CC, and WD repeats predicted to form a β-propeller. (bottom) The construct used for purification of the Mdv1 CC domain includes the MBP fused to 10xHis, the PreScission protease cleavage site (PPCS), and Mdv1 residues 231–299 (CC; MBP-10xHis-PPCS-CC). (B) SDS-PAGE analysis of purified MBP-10xHis-PPCS-CC fusion protein stained with Coomassie brilliant blue (lane 1), PreScission protease–cleaved MBP-10xHis-PPCS + CC (lane 2), and purified CC (lane 3). (C) Sedimentation equilibrium profile of the Mdv1 CC fragment at the indicated initial loading concentrations (open symbols) with the corresponding fit of 16,263 D ($MW_{obs}/MW_{monomer}$ = 1.95). Residuals for the nonlinear least-squared fits are shown below. (D) CD wavelength scan of $CC^{231–299}$ dimer. (E) Crystal structure of $CC^{231–292}$ dimer at a 2.6-Å resolution. Hydrophobic side chains of residues L233, L237, I251, I254, L268, I272, and I275 are shown in magenta.

oligomeric state, and orientation of this domain is important to understand how Mdv1 initially interacts with the Dnm1 dimer and how this interaction positions the Dnm1 dimer for further polymerization.

In this study, we present the structure of the Mdv1 HR, which forms an unusually long (92 Å) antiparallel coiled coil (CC). We also provide a structural model of dimeric Mdv1 bound to two uncomplexed Fis1 molecules anchored at the mitochondrial membrane. This model shows how the CC positions the two β-propeller domains of Mdv1 to interact with Dnm1 as it transitions from the cytoplasm to mitochondria. In vivo experiments indicate that formation of the Mdv1 antiparallel CC and CC length are important for Fis1 binding, Dnm1 recruitment and assembly, coassembly of Mdv1 into the fission complex, and mitochondrial fission. Surprisingly, restoring Mdv1 oligomerization using a heterologous antiparallel CC rescues Dnm1, but not Fis1, interactions. Thus, the sequence of the Mdv1 CC plays an important but unanticipated role in Mdv1–Fis1 binding. Using a substitution exposed at the surface of the CC, we show that the CC sequence can function to stabilize the Mdv1–Fis1 complex. The combined data reveal new insights into the formation of functional mitochondrial fission complexes.

Results

Structure of the Mdv1 CC

The Mdv1 sequence was analyzed using the MultiCoil CC prediction program (Wolf et al., 1997). The ends (231–299) for the expression construct were chosen based on the total probability score (P > 0.2). Mdv1 $CC^{231–299}$ was expressed as a maltose-binding protein (MBP) fusion protein in *Escherichia coli*, released by proteolytic cleavage, and purified to homogeneity (see Materials and methods; Fig. 1, A and B). Equilibrium sedimentation (ES) centrifugation (Fig. 1 C) and circular dichroism (CD) analyses (Fig. 1 D) indicated that Mdv1 $CC^{231–299}$ is a dimer exhibiting double minima typical of a strong α-helix.

Published December 13, 2010

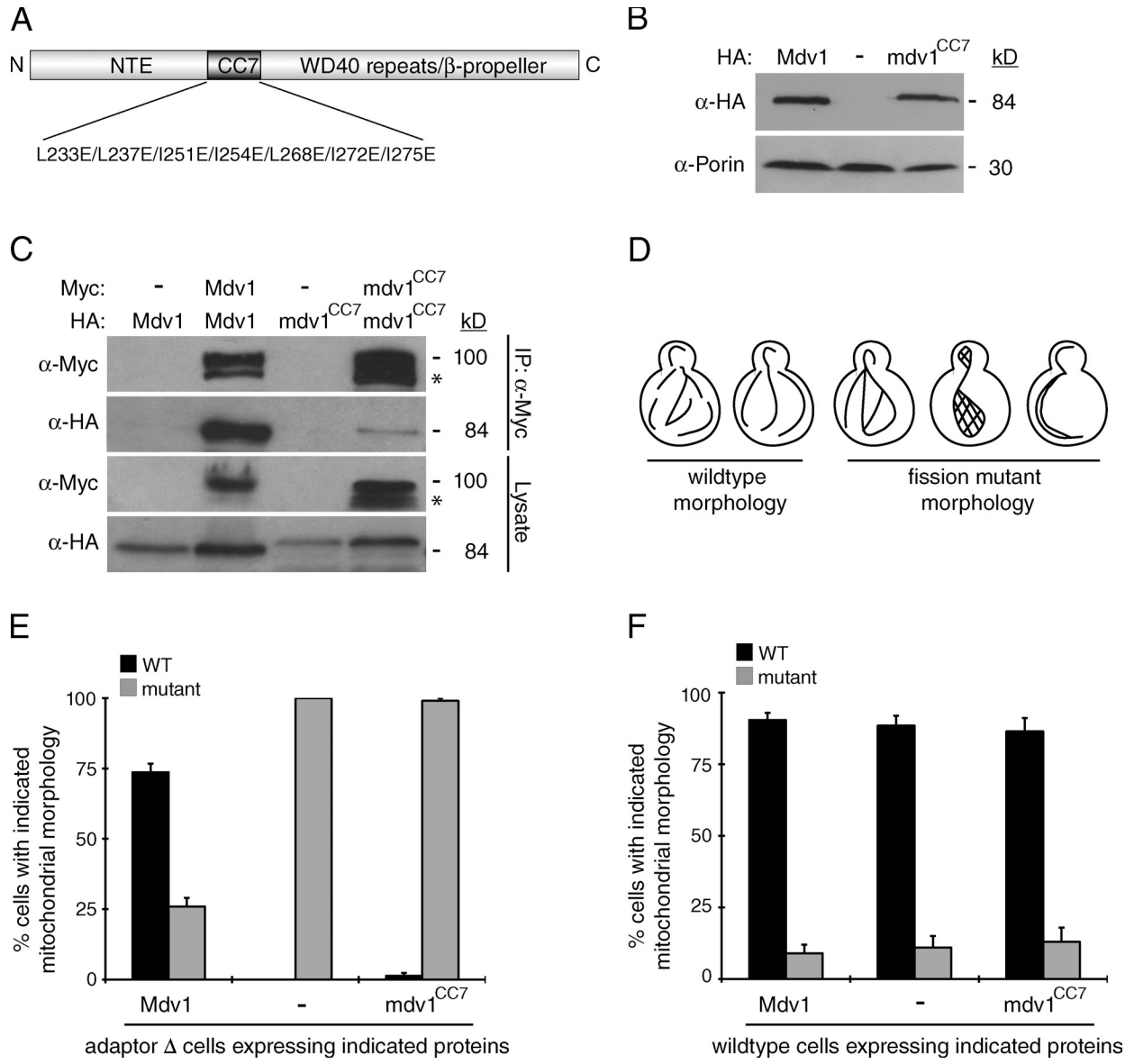

Figure 2. **Disruption of Mdv1 CC formation blocks mitochondrial fission.** (A) Schematic of the mdv1^{CC7} mutant protein. Substitutions introduced at a and d positions in the CC to generate the mdv1^{CC7} mutant protein are listed below the diagram. (B) Steady-state abundance of C-terminal HA-tagged Mdv1 and mdv1^{CC7} mutant proteins expressed in adaptor Δ cells. The mdv1^{CC7} protein sometimes migrates at a higher molecular mass than WT Mdv1 (Figs. 3 A, 4 A, and 6). WCEs separated by SDS-PAGE were immunoblotted with anti-HA and anti-porin antibodies. (C) Lysates from cells expressing the indicated C-terminal Myc- and HA-tagged Mdv1 proteins were used for IP with anti-Myc agarose beads. Lysates (bottom) and immunoprecipitated fractions (top) were analyzed by SDS-PAGE and Western blotting with anti-Myc and anti-HA antibodies. Asterisks mark protein breakdown products. (D) Cartoons depicting mitochondrial morphologies scored in quantification experiments as WT or fission mutant. (E and F) Quantification of mitochondrial morphologies in adaptor Δ (E) or WT (F) cells expressing Mdv1 and mdv1^{CC7} mutant proteins. Black and gray bars and error bars represent the mean and standard deviation of at least three independent experiments (n = 100).

The crystal structure of a selenomethionine-substituted Mdv1 CC$^{231–299}$ construct (L248M and L281M; 2.6 Å; Fig. 1 E and Table S2) revealed that residues 231–292 of this polypeptide fold into a single, 92-Å helix that forms an antiparallel homodimer. This structure is unusual, as intermolecular homodimeric CCs are predominantly parallel. To our knowledge, the structure of only one other homodimeric antiparallel CC of this length (>90 Å) has been reported, also in a protein required for mitochondrial membrane dynamics (Mfn1 HR2, 95 Å; Koshiba et al., 2004). The electrostatic surface of the structure is not highly positive (unpublished data), suggesting that Mdv1 CC$^{231–292}$ does not associate directly with negatively charged lipids exposed at the cytoplasmic face of the outer mitochondrial membrane.

The Mdv1 CC is essential for mitochondrial fission

To determine whether the antiparallel CC interaction in Mdv1 was required for mitochondrial fission, we changed isoleucine and leucine residues contributing to formation of the hydrophobic interface in this structure to glutamate in the full-length protein (Figs. 1 E and 2 A, magenta side chains). Consistent with

Published December 13, 2010

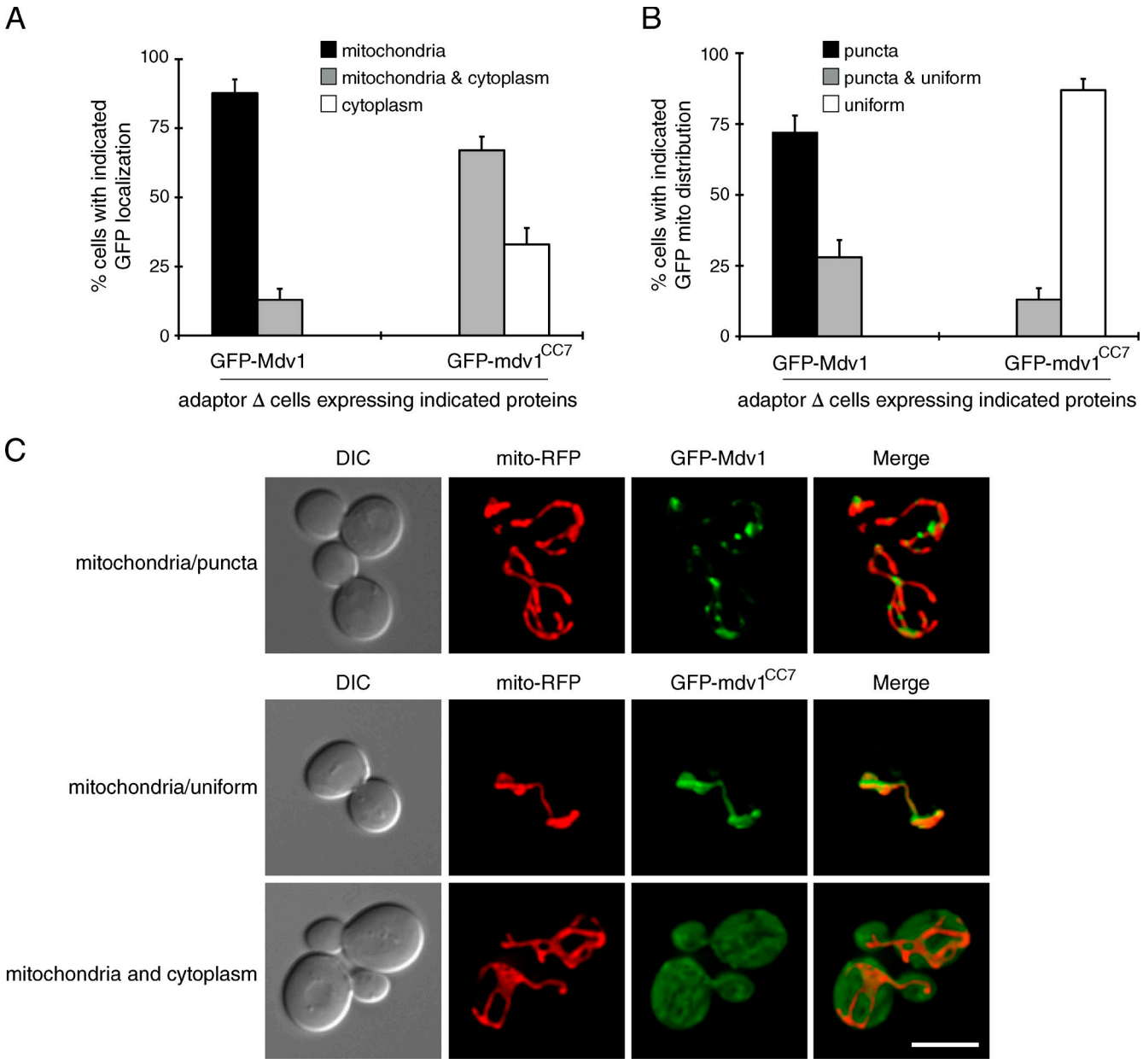

Figure 3. **CC formation promotes mitochondrial recruitment and assembly of the Mdv1 fission adaptor.** (A) Subcellular localization of N-terminal GFP-tagged Mdv1 and mdv1^{CC7} proteins imaged in adaptor Δ cells. (B) Mitochondrial distribution of GFP-tagged Mdv1 and mdv1^{CC7} proteins imaged in adaptor Δ cells. Bars and error bars represent the mean and standard deviation of at least three independent experiments (n = 100). (C) Representative images of GFP-Mdv1 and GFP-mdv1^{CC7} localization and distribution quantified in A and B. DIC, mitochondrial matrix–targeted dsRed (mito-RFP), and merged RFP and GFP images are shown. Bar, 5 µm.

the extended length of this CC, glutamate substitution of all seven isoleucine and leucine residues depicted in Fig. 2 A was necessary to disrupt Mdv1 function (unpublished data). Western blotting of yeast whole cell extracts (WCEs) indicated that the abundance of the mutant adaptor protein, hereafter referred to as mdv1^{CC7}, was similar to that of wild-type (WT) Mdv1 (Figs. 2 B and S4 A). However, these mutations nearly abolished the ability of mdv1^{CC7} to self-interact in coimmunoprecipitation (co-IP) experiments (Fig. 2 C).

We tested the ability of mdv1^{CC7} to support mitochondrial fission in adaptor-null (adaptor Δ) yeast cells lacking Mdv1 and its paralogue Caf4 (Griffin et al., 2005). Although Mdv1 is required for the majority of mitochondrial fission that occurs in vivo, deletion of both Mdv1 and Caf4 is necessary to completely abolish fission. The adaptor Δ strain exhibits severe fission defects, including interconnected, netlike, or collapsed mitochondrial tubules (Fig. 2, D and E). Although expression of Mdv1 restored WT morphology in ∼75% of the population, expression of mdv1^{CC7} failed to rescue fission defects (Fig. 2, D and E). Thus, dimerization of Mdv1 via its antiparallel CC plays a critical role in mitochondrial fission. When expressed from the uninduced *MET25* promoter, steady-state abundance of Mdv1 is fourfold higher than that of Mdv1 expressed from its native promoter (Karren et al., 2005; unpublished data). Although expressing

Published December 13, 2010

fourfold higher levels of mdv1^{CC7} protein did not cause dominant fission defects in WT cells (Fig. 2 F), dominant-negative fission phenotypes began to appear when expression was further elevated by a 4-h induction of the *MET25* promoter (Fig. S4 C, ~16-fold overexpression). This dominant-negative effect suggests that mdv1^{CC7} continues to interact with one or more of its other two binding partners, effectively interfering with the WT fission machinery.

CC formation promotes mitochondrial recruitment and assembly of the Mdv1 fission adaptor

We used the mdv1^{CC7} mutant protein to test the importance of Mdv1 CC formation for its membrane recruitment. Experiments in intact cells expressing GFP-mdv1^{CC7} revealed that the localization of the mutant protein was compromised relative to WT. In control experiments, the majority of WT GFP-Mdv1 colocalized with RFP-labeled mitochondrial tubules (Fig. 3, A and C, top), whereas a small fraction of cells also displayed dual localization to mitochondria and the cytoplasm (Fig. 3 A). In contrast, GFP-mdv1^{CC7} did not localize exclusively with mitochondria. Instead, yeast cells expressing GFP-mdv1^{CC7} exhibited dual mitochondrial and cytoplasmic localization or exclusively cytoplasmic localization of the adaptor protein (Fig. 3, A and C, bottom). Western blotting indicated that this cytoplasmic localization was not caused by proteolysis and release of GFP from the N terminus of the fusion protein (unpublished data).

After membrane recruitment, localization of a subpopulation of Mdv1 appears punctate because of its coassembly with the Dnm1 GTPase into fission complexes (Tieu and Nunnari, 2000; Cerveny et al., 2001; Griffin et al., 2005; Karren et al., 2005; Naylor et al., 2006). Although mitochondrial localized GFP-Mdv1 was largely punctate (Fig. 3 B), GFP-mdv1^{CC7} failed to coassemble into punctate fission complexes and uniformly labeled mitochondrial membranes in the majority of cells (Fig. 3, B and C, middle). This uniform mitochondrial labeling resulted from association of Mdv1 with Fis1 and was abolished in cells lacking Fis1 (mdv1^{CC7} had no effect on Fis1 localization; unpublished data). These combined data indicate that CC formation promotes both Mdv1 recruitment to Fis1 on mitochondria and subsequent higher order assembly of Mdv1 into fission complexes.

Mitochondrial recruitment and self-assembly of the Dnm1 GTPase requires Mdv1 CC formation

The Dnm1 GTPase interacts with the C terminus of Mdv1 (Tieu et al., 2002; Cerveny and Jensen, 2003), which is predicted to form a multibladed β-propeller. This interaction promotes the self-assembly of Dnm1 into rings and spirals (Lackner et al., 2009) that are visualized as mitochondrial puncta (fission complexes) when labeled with a fluorescent marker (Otsuga et al., 1998). We tested whether Mdv1 dimerization in vivo was required for Mdv1–Dnm1 interaction and Dnm1 assembly into mitochondrial puncta. Although HA-tagged Mdv1 efficiently coprecipitated Dnm1 from cell lysates, complex formation between mdv1^{CC7}-HA and Dnm1 was significantly reduced (Fig. 4 A). This reduced interaction was also apparent in vivo. Although GFP-Dnm1 efficiently assembled into puncta on mitochondria when cells expressed WT Mdv1 (Fig. 4, B and C, top), the fraction of cytoplasmic GFP-Dnm1 increased in cells expressing mdv1^{CC7} (Fig. 4, B and C, bottom). Residual GFP-Dnm1 puncta on mitochondria in mdv1^{CC7}-expressing cells were often smaller and less-evenly distributed on the organelle tubules (Fig. 4 C, middle). This may be caused in part by the fact that mdv1^{CC7} uniformly labels mitochondrial membranes (RFP-mdv1^{CC7}; Fig. 4 D) but does not efficiently coassemble into puncta with Dnm1 (Fig. 3 C, middle and bottom). When combined with our finding that GFP-mdv1^{CC7} fails to form mitochondrial puncta and cannot support fission (Fig. 2 E; and Fig. 3 C, middle and bottom), these results provide a direct demonstration that dimeric Mdv1 must coassemble with the Dnm1 GTPase to form functional fission complexes.

Mdv1 dimerization via a heterologous antiparallel CC partially restores adaptor function

To determine whether physical CC formation was sufficient for adaptor function, we generated a chimeric protein, which replaced the Mdv1 CC with residues 674–734 of the mammalian mitofusin protein Mfn1 (mdv1^{HR2}; Fig. 5 A). In crystallographic experiments, this Mfn1 domain forms an antiparallel CC similar in length to the Mdv1 CC (95 Å; Koshiba et al., 2004). As observed for WT Mdv1, the mdv1^{HR2} chimera was stably expressed (Figs. 5 B and S4 A), localized with mitochondria in differential fractionation and fluorescence microscopy experiments (Figs. 5 C and S1 A), and was able to self-interact in co-IP experiments (Fig. 5 D). Unlike WT Mdv1, mdv1^{HR2} only partially rescued mitochondrial fission and morphology defects in the adaptor Δ strain (Figs. 5 E and S1 B). This partial rescue could not be attributed to defects in mdv1^{HR2}–Dnm1 interactions because mdv1^{HR2}-HA coimmunoprecipitated Dnm1 and the WT adaptor (Fig. 5 F), formed mitochondrial puncta in vivo when labeled with GFP (Fig. S1 C), and also promoted assembly of GFP-Dnm1 into punctate mitochondrial fission complexes (Fig. S1 D). These results were surprising because they suggested that dimerization of Mdv1 via an antiparallel CC is important but not sufficient for the adaptor's function in mitochondrial fission. Instead, the sequence of the Mdv1 CC may also contribute to adaptor function.

The sequence of the Mdv1 CC is critical for interaction with Fis1

We noticed that the mitochondrial localization of mdv1^{HR2} decreased relative to Mdv1 when Dnm1 was absent (Fig. S1 E). Under these conditions, stable mitochondrial association of mdv1^{HR2} depends entirely upon interactions with Fis1. Thus, the inability of mdv1^{HR2} to fully rescue fission defects in vivo could result from a reduced Fis1 interaction. It has been unclear whether the Mdv1 CC is necessary for interaction with Fis1. A crystal structure showed that α-helices in the N-terminal extension (NTE) of fission adaptor proteins bind directly to the cytoplasmic tetratricopeptide domain of Fis1 (Zhang and Chan, 2007). Mutations predicted to disrupt contact sites in this complex interfered with Mdv1–Fis1 interactions and reduced fission in vivo.

Published December 13, 2010

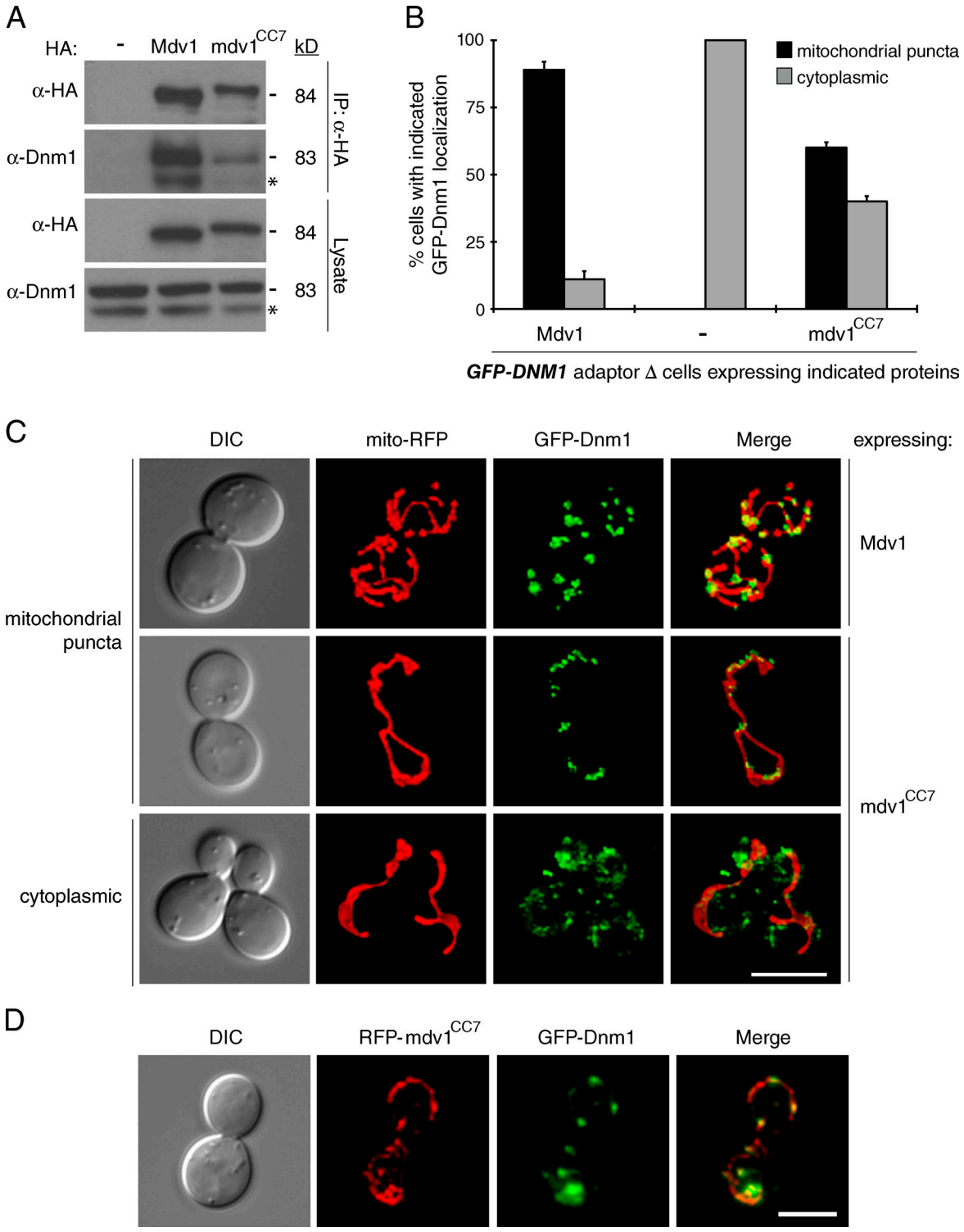

Figure 4. **Efficient Dnm1–Mdv1 interaction and Dnm1 assembly into functional mitochondrial fission complexes requires Mdv1 CC formation.** (A) Lysates from cells expressing the indicated C-terminal HA-tagged Mdv1 proteins were used for IP with anti-HA agarose beads. Lysate (bottom) and immunoprecipitated fractions (top) were analyzed by SDS-PAGE and Western blotting with anti-HA and anti-Dnm1 antibodies. Asterisks mark protein breakdown products. (B) Localization of genomically expressed GFP-Dnm1 in cells expressing Mdv1 or mdv1^{CC7}. Bars and error bars represent the mean and standard deviation of at least three independent experiments (n = 100). (C) Representative images of GFP-Dnm1 localization quantified in B. DIC, mitochondrial matrix–targeted RFP (mito-RFP), GFP-Dnm1, and merged RFP and GFP images are shown. (D) Colocalization of RFP-mdv^{CC7} and GFP-Dnm1. DIC and merged RFP with GFP images are shown. Bars, 5 µm.

However, genetic suppressor experiments from our laboratory suggested that the Mdv1 CC also contributes to the Mdv1–Fis1 interaction. We previously screened for suppressors of a Fis1 protein–destabilizing mutation (*fis1-3*; Karren et al., 2005). *fis1-3* contains E78D, I85T, and Y88H substitutions in the concave surface of the Fis1 TPR domain that destabilize the protein at an

Published December 13, 2010

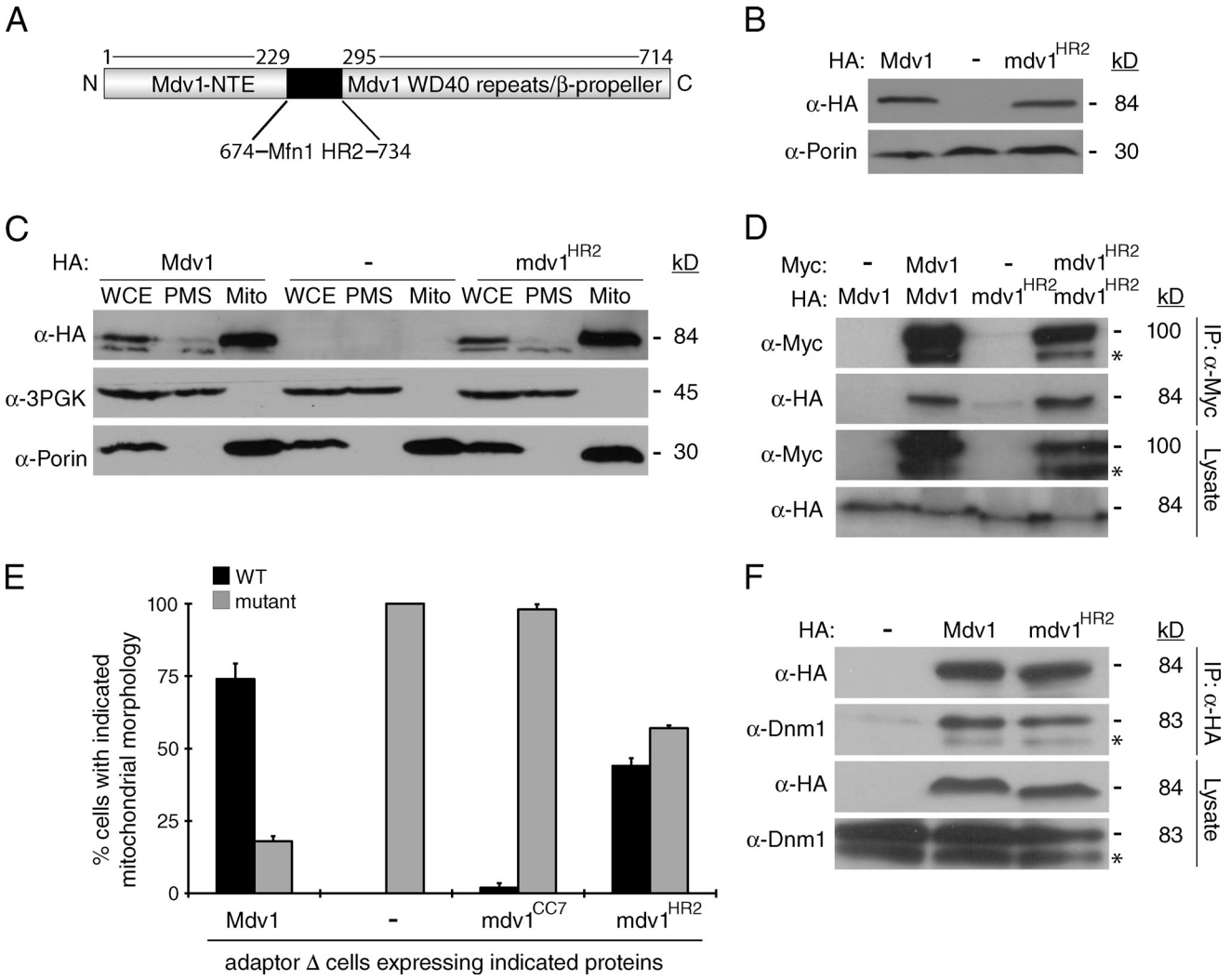

Figure 5. **Dimerization via a heterologous antiparallel CC partially restores Mdv1 adaptor function.** (A) Schematic representation of the mdv1^{HR2} chimera. Residues 230–294 encompassing the Mdv1 antiparallel CC are replaced by residues 674–734 of the Mfn1 HR2 domain. (B) Steady-state abundance of C-terminal HA-tagged Mdv1 and mdv1^{HR2} mutant proteins expressed in fission adaptor Δ cells. WCEs separated by SDS-PAGE were immunoblotted with anti-HA and anti-porin antibodies. (C) Differential sedimentation and Western blot analysis of cytoplasmic 3PGK, mitochondrial porin, and HA-tagged Mdv1 and mdv1^{HR2} proteins in WCE, postmitochondrial supernatant (PMS), and mitochondrial (Mito) fractions. (D) Lysates from cells expressing the indicated C-terminal Myc- and HA-tagged Mdv1 and mdv1^{HR2} proteins were used for IP with anti-Myc agarose beads. Lysate (bottom) and immunoprecipitated fractions (top) were analyzed by SDS-PAGE and Western blotting with anti-HA and anti-Myc antibodies. (E) Quantification of mitochondrial morphologies in adaptor Δ cells expressing Mdv1, mdv1^{CC7} mutant, or mdv1^{HR2} chimeric proteins. Bars and error bars represent the mean and standard deviation of at least three independent experiments (n = 100). (F) Lysates from cells expressing HA-tagged Mdv1 or mdv1^{HR2} were used for IP with anti-HA agarose beads. Lysates (bottom) and immunoprecipitated fractions (top) were analyzed by SDS-PAGE and Western blotting with anti-HA and anti-Dnm1 antibodies. Asterisks mark protein breakdown products.

elevated temperature (37°C). We identified an E250G substitution in the Mdv1 CC domain (at position g in the HR; Fig. S2) that stabilized Mdv1–Fis1 complex formation and restored mitochondrial fission at 37°C in the *fis1-3* strain. These findings strongly suggest that the CC sequence is important for Mdv1–Fis1 interaction. To test this idea, we examined the ability of mdv1^{HR2} to interact with Fis1. As shown in Fig. 6, Myc-tagged Fis1 efficiently coprecipitated HA-tagged Mdv1 from cell lysates, whereas coprecipitation of the CC defective mdv1^{CC7}-HA protein was reduced. Significantly, coprecipitation of mdv1^{HR2}-HA with Myc-Fis1 was also reduced despite the fact that this chimeric adaptor protein can self-interact via the heterologous Mfn1 HR2 domain. Quantification of these Fis1–Mdv1 coIP interactions confirmed that Fis1 complex formation with mdv1^{CC7} and mdv1^{HR2} proteins are reduced, whereas Fis1 interaction with the mdv1^{E250G} suppressor is enhanced relative to WT (Fig. 6 B). The straightforward interpretation of these results is that the sequence of the Mdv1 CC (and not just its dimerization capability) is critical for Mdv1 binding to Fis1 during early steps in fission complex assembly.

The length of the Mdv1 CC is optimized for mitochondrial fission

To test the influence of CC length on Mdv1 function, we generated variants lacking two (mdv1$^{\Delta 2HR}$) or four (mdv1$^{\Delta 4HR}$) HRs of the native Mdv1 CC (Fig. 7 A). Both ΔHR proteins were stably expressed at similar steady-state abundance, continued to self-interact, localized to mitochondria in a Fis1-dependent manner,

Published December 13, 2010

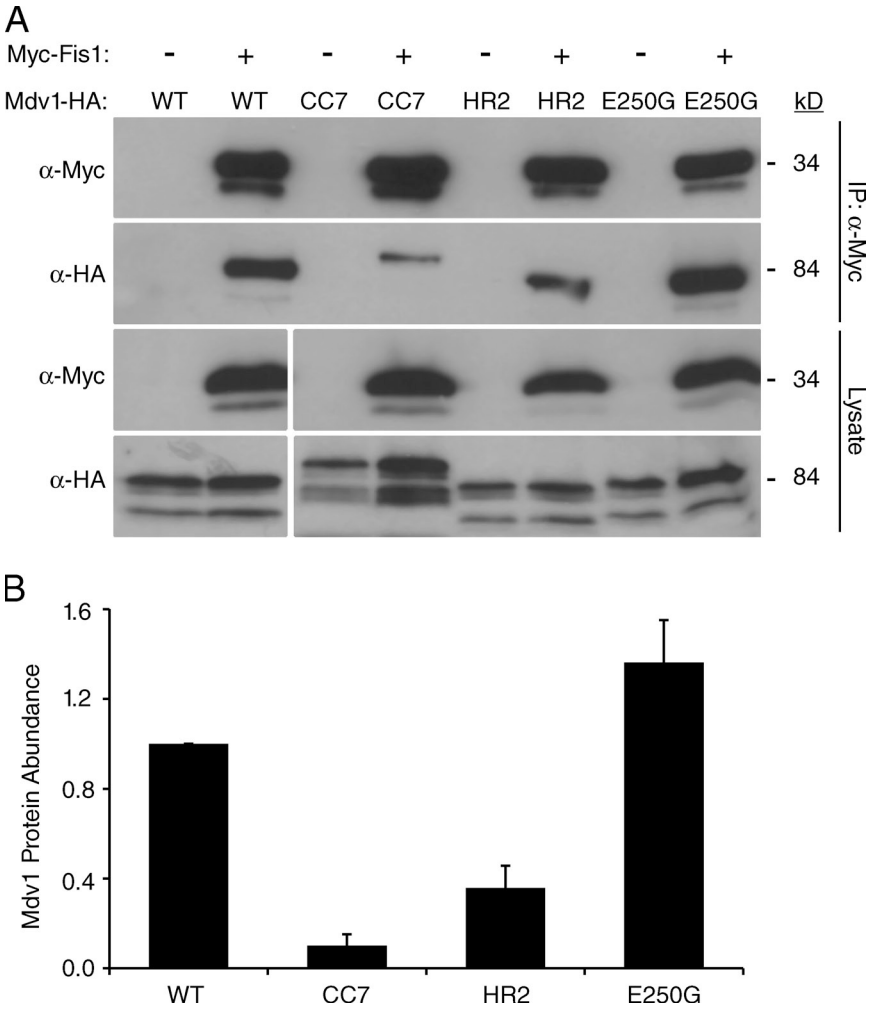

Figure 6. **The Mdv1 CC sequence contributes to efficient Fis1 binding.** (A) Lysates from cells expressing the indicated Mdv1-HA variants and Myc-Fis1 were used for coIP with anti-Myc agarose beads. Lysate (bottom) and IP fractions (top) were analyzed by SDS-PAGE and ECL Western blotting with anti-HA and anti-Myc antibodies. Lower molecular mass bands in all lanes are protein breakdown products. (B) Quantification of coIPs shown in A. Myc- and HA-tagged proteins were detected using a fluorescent secondary antibody followed by scanning on an imaging system. The mean intensity of each Mdv1-HA protein band was normalized to the Myc-Fis1 signal in the same coIP. Bars represent the abundance of Mdv1-HA signal in each coIP relative to the WT. Error bars represent the mean and standard deviation from three independent experiments.

and promoted Dnm1 assembly into mitochondrial fission complexes in vivo (Fig. S3, A, B, and D; Fig. S4, A and B; and not depicted). However, the ΔHR Mdv1 variants did not form mitochondrial puncta as efficiently as WT Mdv1 and exhibited increased uniform labeling of mitochondrial tubules (Fig. S3 C). Moreover, neither ΔHR protein rescued fission defects in the adaptor Δ strain and WT (Fig. 7 B). Thus, the ΔHR Mdv1 variants have a reduced ability to assemble and function in fission. Like the mdv1^{CC7} mutant, the ΔHR variants continued to interact with binding partners in vivo and caused dominant-negative fission defects when overexpressed in a WT strain (Fig. S4 C and not depicted). The dominant-negative defects induced by the ΔHR variants were more severe than those caused by overexpression of mdv1^{CC7} or WT Mdv1, indicating that they have greater ability to interfere with the WT fission machinery in vivo.

We also compared the ability of the ΔHR and E250G Mdv1 variants to restore mitochondrial fission at 25°C and 37°C in cells harboring the *fis1-3* allele. In the *fis1-3 mdv1Δ* strain grown at an elevated temperature, mitochondrial fission is rescued by expression of Mdv1^{E250G} but not WT Mdv1 (Fig. 7 C). The mdv1$^{\Delta 2HR}$ and mdv1$^{\Delta 4HR}$ proteins rescued mitochondrial fission defects at 37°C but less efficiently than Mdv1^{E250G}. In addition, neither mdv1$^{\Delta 2HR}$ nor mdv1$^{\Delta 4HR}$ rescued fission defects and WT or Mdv1^{E250G} at the permissive temperature (25°C).

As with mdv1^{HR2}, we observed that mitochondrial localization of mdv1$^{\Delta 2HR}$ and mdv1$^{\Delta 4HR}$ decreased relative to WT Mdv1 in cells lacking Dnm1 (unpublished data). Because Mdv1 mitochondrial localization in *dnm1Δ* is Fis1 dependent, it is likely that shortening the native Mdv1 CC domain compromises the Fis1–Mdv1 interaction. Based on these combined results, we conclude that the overall length of the native CC is optimized for Mdv1 adaptor function in mitochondrial fission complex assembly and fission.

Discussion

Mdv1 is essential for the membrane recruitment and assembly of the mitochondrial dynamin Dnm1. By combining the new structure of the Mdv1 CC domain with a previously reported Fis1–Mdv1 NTE structure (Zhang and Chan, 2007), we provide a working model for the architecture of the Fis1–Mdv1 complex on the membrane. As depicted in Fig. 8, formation of a 92-Å antiparallel CC between two Mdv1 polypeptides forms an extended dimer. The NTE of each Mdv1 subunit is bound to distinct Fis1 TPR-like domains exposed at the cytoplasmic face of the mitochondrial membrane. Cryo-EM structures suggest that dimeric Dnm1 is the basic subunit for assembly of Dnm1 spirals (Hinshaw, J., personal communication), and two-hybrid

Published December 13, 2010

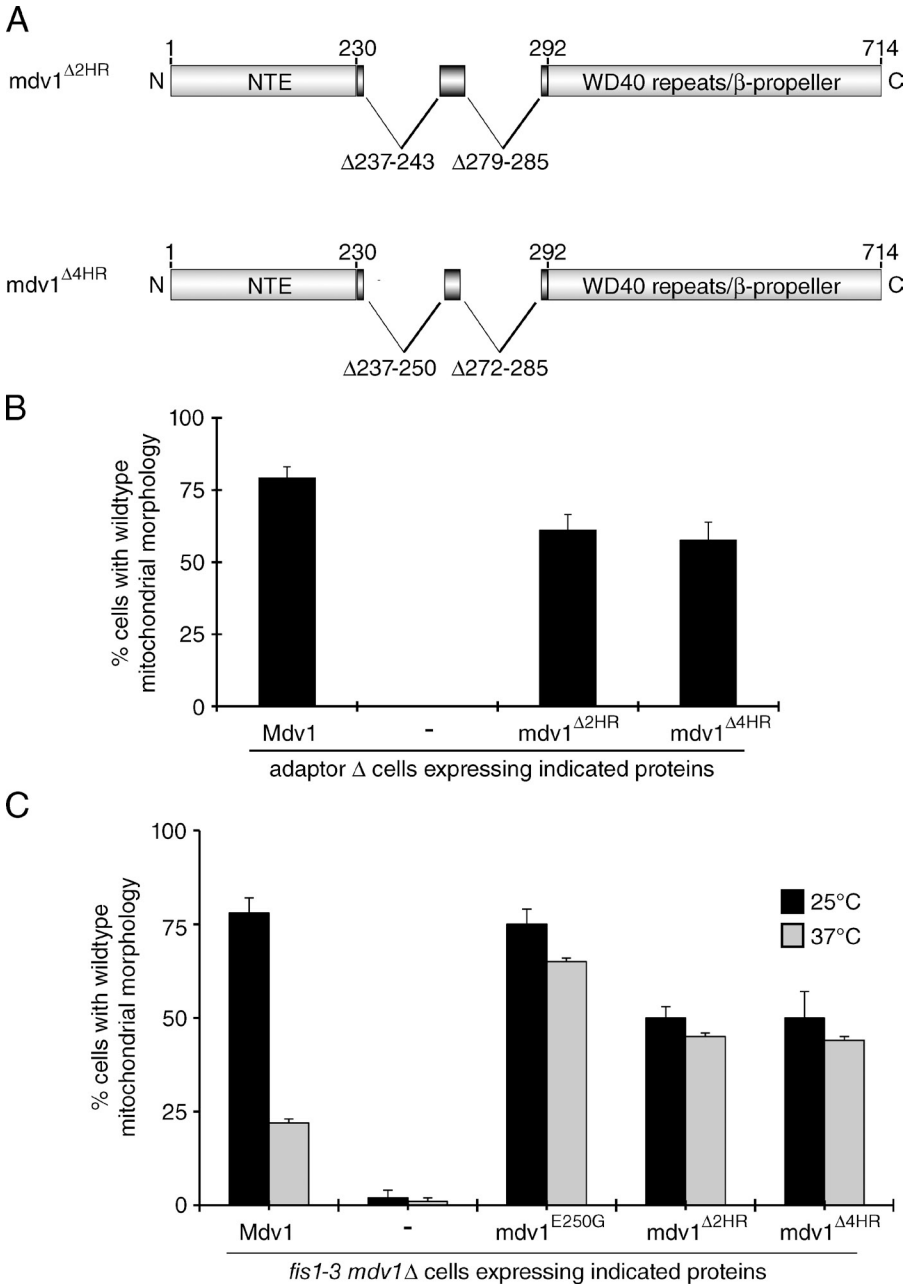

Figure 7. **Effect of CC shortening on Mdv1 function.** (A) Schematic of the mdv1$^{\Delta 2HR}$ and mdv1$^{\Delta 4HR}$ proteins. Residues corresponding to HR deletions are shown below each diagram. (B) Quantification of mitochondrial morphologies in adaptor Δ cells expressing Mdv1, mdv1$^{\Delta 2HR}$, and mdv1$^{\Delta 4HR}$ proteins. (C) Quantification of mitochondrial morphologies at 25 and 37°C in *fis1-3 mdv1Δ* cells expressing WT and mutant Mdv1 proteins. Black and gray bars and error bars represent the mean and standard deviation of at least three independent experiments (n = 100).

and co-IP analyses indicate that the predicted Mdv1 β-propeller domain is sufficient for Dnm1 interaction (Tieu et al., 2002; Cerveny and Jensen, 2003). Thus, Mdv1 β-propeller domains at each end of the CC would provide interaction sites for dimeric Dnm1 recruited from the cytoplasm. Dnm1 dimer binding could occur at the periphery or on the lateral face of one or multiple Mdv1 β-propeller domains. Alternatively, each Mdv1 dimer could bind a single Dnm1 dimer, as suggested by the ∼1:1 Mdv1–Dnm1 stoichiometry of complexes assembled in vitro (Lackner et al., 2009). Previous studies identified residues in the Mdv1 β-propeller important for Dnm1 interaction (Cerveny and Jensen, 2003; Naylor et al., 2006); however, it is not known whether these residues make direct contact with Dnm1. Identification of such contact sites and/or structures of protein complexes will be necessary to model Mdv1–Dnm1 binding and determine how this interaction positions Dnm1 dimers to facilitate assembly into spirals. Although the overall length of the native Mdv1 CC is optimized for fission complex assembly and function, our experiments of the ΔHR mdv1 variants indicate that maintaining the length of this CC is not essential for Mdv1 function.

In addition to providing structural stability, Mdv1 dimerization via the CC is critical for the accurate assembly of functional Dnm1 fission complexes. The fraction of monomeric mdv1^{CC7} protein that localizes to mitochondria is sometimes sufficient to recruit and promote the assembly of Dnm1 puncta that resemble fission complexes (Fig. 4 C). However, the morphology of these structures is often qualitatively different from those observed in WT cells, as is their distribution along the mitochondrial tubule. Unlike WT Mdv1, which coassembles with Dnm1 during formation of a functional fission complex,

Published December 13, 2010

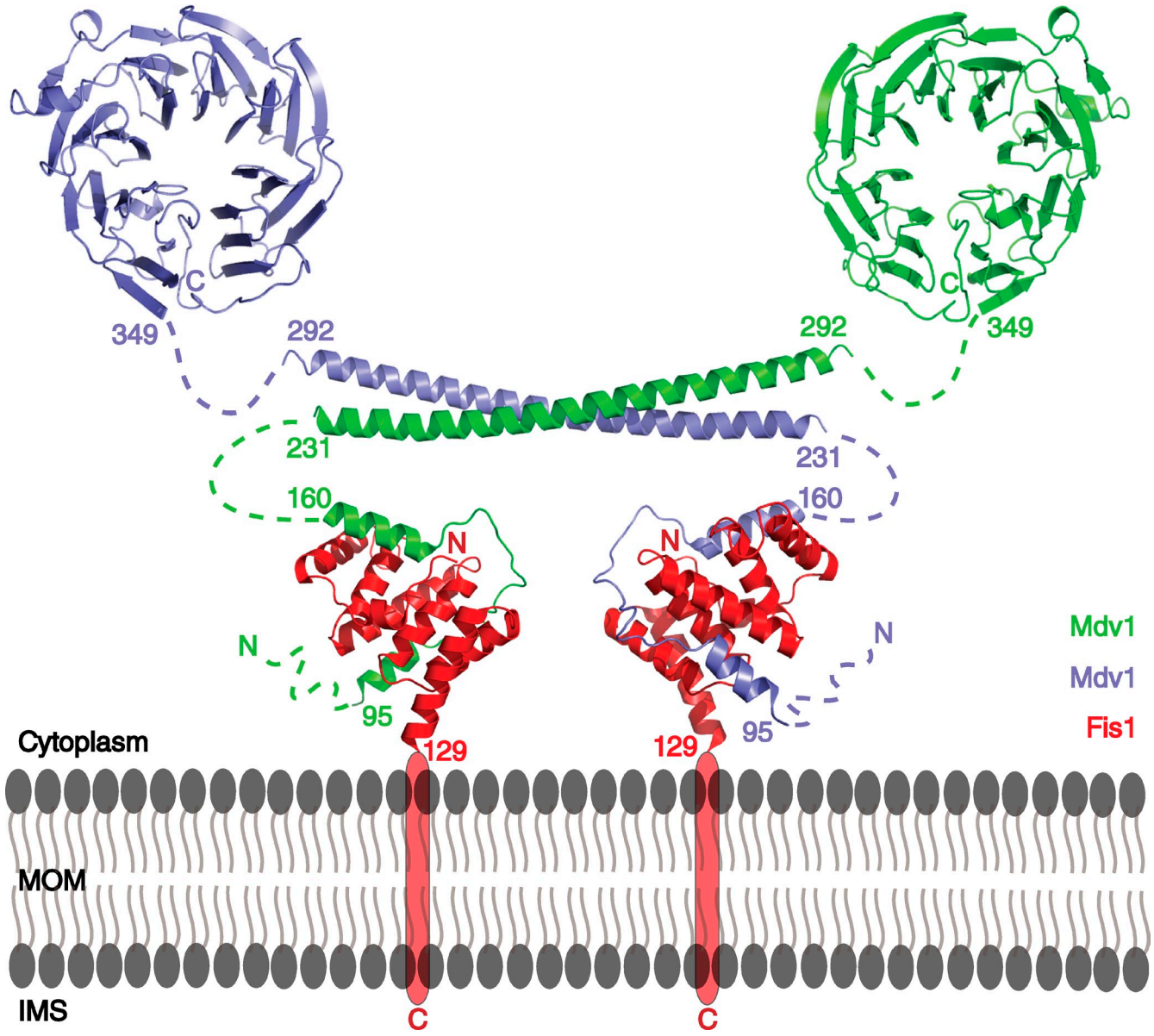

Figure 8. **Molecular architecture of the mitochondrial dynamin-related receptor.** A structural model of the Mdv1 dimer (green/purple) bound to two Fis1 cytoplasmic domains (red) anchored in the outer mitochondrial membrane (gray). The model was generated from crystal structures of the Fis1 cytoplasmic domain in complex with a fission adaptor NTE (Protein Data Bank [PDB] accession no. 2PQR) and the Mdv1 antiparallel CC (PDB accession no. 2XU6). The C-terminal WD40 domain of Mdv1 is shown as a homology model based on the known structure of the Cdc4 WD40 repeat (PDB 1NEX). Loops of variable length and unknown structure connect these two regions to the central CC dimer.

mdv1^{CC7} fails to assemble and form visible puncta in vivo (Fig. 4 D). This last observation is consistent with the idea that a scaffolding function of dimeric Mdv1 is necessary for its inclusion in the Dnm1 polymer as it assembles. The scaffolding model is also supported by our finding that restoring Mdv1 dimerization using a heterologous antiparallel CC rescues mdv1^{HR2} oligomerization and mitochondrial fission defects.

Surprisingly, the rescue provided by mdv1^{HR2} was incomplete, owing to a reduction in the interaction of the chimeric protein with Fis1 (Fig. 6). This result complements our previous finding that an E250G CC substitution stabilizes complex formation between Mdv1 and both WT and mutant Fis1 proteins (Karren et al., 2005). Glu250 lies at heptad position g in the native CC (Fig. S2) and likely participates in an electrostatic interaction that stabilizes a protein–protein interface. In additional experiments, we have shown that mdv1^{E250G} and mdv1^{E250A} substitutions suppress fission defects caused by a mutant Fis1 protein equally well (unpublished data). The E to G substitution is predicted to increase helix flexibility in addition to disrupting a side chain interaction. The E to A substitution should not increase helix flexibility but could also disrupt a side chain interaction. The simplest explanation for these combined findings is that Mdv1 Glu250 negatively regulates Fis1 binding via an Mdv1 self-interaction or interaction with another protein. According to this scenario, both the E to G and E to A substitutions would disrupt this interaction, generating a form of Mdv1 that is constitutively available for partner binding. Because the exact nature of this interaction remains to be determined, it is

Published December 13, 2010

not depicted in Fig. 8. A simple binding interface between Fis1 and Mdv1 seems unlikely, as the purified Fis1 cytoplasmic domain is not able to bind the purified Mdv1 CC in vitro (unpublished data).

Fis1–Mdv1 is the only membrane-anchored receptor complex known to function with a dynamin-related GTPase in a membrane fission event. Our experiments provide the first structural model for the presentation of binding sites recognized by the Dnm1 GTPase as it transitions from the cytoplasm to the mitochondrial outer membrane. Although the Fis1–Mdv1 complex is uniformly distributed on the membrane, assembly of Dnm1 and Mdv1 into fission complexes is restricted to discrete sites along the length of the mitochondrial tubule. Thus, post-translational modifications and/or induced conformation changes in the Fis1–Mdv1 complex seem essential to regulate Dnm1 access to the Mdv1 β-propellers. Alternatively, additional factors may act in vivo to stabilize Dnm1 assembly at specific locations and limit its propagation laterally on the membrane. Our results provide a framework for understanding how adaptors act as scaffolds to orient and stabilize the assembly of dynamins on membranes.

Materials and methods

Protein production

Mdv1 residues 231–299 (Mdv1-CC) were fused to the C terminus of MBP via a linker containing 10xHis and the PreScission protease cleavage site (MBP-10xHis-PPCS-CC$^{231–299}$). This construct was expressed in BL21(DE3) codon$^+$ (RIPL; Agilent Technologies) *E. coli* grown in autoinduction medium (Studier, 2005). Overnight cultures, grown in PA-0.5G, were diluted (1:1,000) in ZYP-5052 (MBP-CC) or PASM-5052 (MBP-CC^{SeMet}) and grown at 37°C for 8 h (Studier, 2005). Cultures were transferred to 23°C and grown for an additional 12–36 h before harvesting. All purification steps were performed at 4°C. Proteins were purified by affinity chromatography on amylose resin (New England Biolabs, Inc.) followed by cleavage with PreScission protease (GE Healthcare). After cleavage, Mdv1-CC contained two heterologous N-terminal residues (Gly-Pro). Protein was further purified by mono-Q anion exchange chromatography (GE Healthcare). Residual MBP and uncleaved protein were removed by additional nickel Sepharose (GE Healthcare) and amylose affinity chromatography. Purified Mdv1-CC was dialyzed in CD/ES buffer (50 mM Na-phosphate, pH 7.4, and 150 mM NaCl) or crystallization buffer (20 mM Tris-Cl, pH 7.5, and 100 mM NaCl) and concentrated to 1–10 mg/ml using Centriprep centrifugal concentrators (YM-3; 3 kD NMWL; Millipore).

CD and ES analysis

CD analysis was performed on a CD spectrometer (410; Aviv Biomedical, Inc.). Wavelength scans (200–260 nm) were performed at 23°C on 10 µM protein samples in 50 mM sodium phosphate, pH 7.4, and 150 mM NaCl using a 1-mm path length cuvette with a 5-s averaging time. ES analysis of Mdv1-CC was performed at 4°C using a centrifuge (Optima XL-A; Beckman Coulter) at initial protein subunit concentrations of 335.0, 168.0, and 84.0 µM (monomer) in a buffer containing 50 mM sodium phosphate, pH 7.4, and 150 mM NaCl. Centrifugation was performed at 20,000 rpm (Fig. 1 C) and 25,000 rpm. Resulting equilibrium datasets were globally fit to a single ideal species model with a floating molecular mass using the nonlinear least-squares algorithms in HeteroAnalysis software (Cole, 2004). Protein partial–specific volumes and solvent densities were calculated with the program SEDNTERP (version 1.09; Laue et al., 1992).

Crystallization and structure determination

The protein crystallized in several conditions of the Crystal Screen HT (Hampton Research). After optimization, Mdv1-CC^{SeMet} (10 mg/ml in 20 mM Tris-Cl, pH 7.5, and 100 mM NaCl) was crystallized in 2 µl/2 µl vapor diffusion experiments against a well solution containing 16% PEG 3350, 0.1 M Bis-Tris-Propane, pH 7.5, and 0.4 M NaCl. Flat-plate crystals were cryoprotected in 20% PEG 3350, 0.1 M BTP, pH 7.5, 0.4 M NaCl, and 25% glycerol and flash frozen in liquid nitrogen. Peak and inflection data were collected on beamline (version 7.1; SSRL) and processed with HKL2000 (Otwinowski and Minor, 1997) to a final Rmerge of 5.3% to 2.6 Å. The selenium sites were identified with SOLVE (Terwilliger and Berendzen, 1999), and solvent flattening and preliminary model building with RESOLVE (Terwilliger and Berendzen, 1999) resulted in 60% of the residues correctly positioned. Final model building and validation was performed in COOT (Emsley and Cowtan, 2004). Refinement with REFMAC5 (Murshudov et al., 1997) within the CCP4 suite (Collaborative Computational Project 4, 1994) resulted in a final R_{factor}/R_{merge} of 27.1%/31.1% and a model with good geometric statistics (Table S2).

Yeast strains and plasmids

Yeast strains used in this study include JSY5740 (*MATa leu2Δ1 his3Δ200 trp1Δ63 ura3-52 lys2Δ202*), JSY8612 (*MATa leu2Δ1 his3Δ200 trp1Δ63 ura3-52 lys2Δ202 mdv1::HIS3 caf4::KanMX*; also referred to as the adaptor Δ strain), JSY9465 (*MATa leu2Δ1 his3Δ200 trp1Δ63 ura3-52 lys2Δ202 mdv1::HIS3 caf4::KanMX dnm1::GFP-DNM1*), JSY9135 (*MATa leu2Δ1 his3Δ200 trp1Δ63 ura3-52 lys2Δ202 mdv1::HIS3 caf4::KanMX dnm1::HIS3*), JSY9541 (*MATa leu2Δ1 his3Δ200 trp1Δ63 ura3-52 lys2Δ202 mdv1::HIS3 caf4::KanMX fis1::HIS3*), and JSY7674 (*MATa leu2Δ1 his3Δ200 trp1Δ63 ura3-52 fis1-3 mdv1::HIS3*).

A list of plasmids used in this study is provided in Table S1. To construct *pMAL-c2x-mdv1-CC*, DNA sequences encoding residues 231–299 of *MDV1* were PCR amplified with a forward primer that introduced an EcoRI site, 10xHis, a PreScission Protease cleavage site, and a reverse primer that introduced three stop codons and a HindIII site. The resulting fragment was cloned into the EcoRI and HindIII sites of the *pMAL-c2x* vector (New England Biolabs, Inc.). The *pMAL-c2x-mdv1-CC^{SeMet}* construct was made by site-directed mutagenesis (QuikChange kit; Agilent Technologies) of *pMAL-c2x-mdv1-CC* to change leucine codons to methionine codons at positions encoding residues 248 and 281 in the full-length Mdv1 protein. Construction of *pRS416MET25-MDV1* was described previously (Karren et al., 2005). For *pRS416MET25-mdv1^{CC7}*, sequential site-directed mutagenesis of a p*RS416MET25-MDV1* template was used to introduce sequences encoding the substitutions L233E, L237E, I251E, I254E, L268E, I272E, and I275E. For *pRS415MET25-GFP-MDV1*, pRS415MET25-*GFP-mdv1^{CC7}*, and *pRS415MET25-GFP-mdv1^{HR2}*, PCR-amplified *MDV1*, *mdv1^{CC7}*, and *mdv1^{HR2}* sequences were cloned into the BamHI and SalI sites of *pRS415MET25-GFP*. *pRS415MET25-mdv1^{HR2}* was created using the following five steps: (1) sited-directed mutagenesis was used to introduce two silent restriction endonuclease sites into *MDV1* at nucleotides 628–633 (XmaI) and nucleotides 901–906 (XhoI) in the *pRS416MET25-MDV1* vector, (2) an existing XhoI site in the multiple-cloning site of *pRS416MET25-MDV1* was removed by site-directed mutagenesis, (3) A *$_{yeast}$MDV1-$_{mouse}$MFN1* CC chimeric sequence was synthesized by MR. GENE. The nucleotide sequence of the synthesized *MDV1-MFN1* CC chimera was *XmaI-MDV1(634–687)-MFN1(2022–2202)-MDV1 (883–900)-XhoI*, (4) the CC chimera provided in a vector was excised by XmaI and XhoI digestion and cloned into the same sites of the *pRS416MET25-MDV1* plasmid generated in step 1. To construct, *pRS416MET25-MDV1-13MYC*, *MDV1* was PCR amplified, digested with SpeI and SacII, and cloned into a vector that fused sequence encoding13MYC in frame at the C terminus of Mdv1. *pRS416MET25-mdv1^{CC7}-13MYC* and *pRS416MET25-mdv1^{HR2}-13MYC* were cloned by similar strategies. To create *pRS415MET25-MDV1-3HA*, *MDV1* was PCR amplified, digested, and cloned into the BamHI–XhoI sites of *pRS415MET25-CAF4-3HA*. In the resulting clone, the *CAF4* ORF was replaced by the *MDV1* ORF, and sequence encoding 3HA was fused in frame to the C terminus of Mdv1. A similar strategy was used to generate clones encoding C-terminal 3HA -agged forms of mdv1^{CC7}, mdv1^{HR2}, and mdv1^{E250G}. For *pRS416MET25-9MYC-FIS1*, *9MYC-FIS1* was excised from *pRS415MET25-9MYC-FIS1* (Karren et al., 2005) using SpeI and XhoI and cloned into *pRS416MET25*. To create *pRS416MET25-mdv1^{Δ2HR}* and *pRS416MET25-mdv1^{Δ4HR}*, DNA encoding mdv1^{Δ2HR} (XmaI-634–708-ΔHR-730–836-ΔHR-855–900-XhoI) or mdv1^{Δ4HR} (XmaI-634–708-ΔΔHR-751–813-ΔΔHR-855–900-XhoI) was synthesized and cloned by Integrated DNA Technologies, Inc. After digestion of the provided plasmids with XmaI and XhoI, the cloned fragments were ligated into silent XmaI and XhoI sites engineered on either side of the encoded Mdv1 CC in *pRS416MET25-MDV1*. *pRS415MET25-mdv1^{Δ2HR}-3HA*, *pRS415MET25-mdv1^{Δ4HR}-3HA*, *pRS415MET25-GFP-mdv1^{Δ2HR}*, and *pRS415MET25-GFP-mdv1^{Δ4HR}* were generated using strategies similar to those described for WT and mutant Mdv1 variants. For *pRS416MET25-ffRFP-mdv1^{CC7}*, a PCR-amplified fragment containing mdv1^{CC7} was digested with BamHI and SalI and ligated into *pRS416MET25-ffRFP*.

Published December 13, 2010

Fluorescence microscopy

Mitochondrial morphologies were scored in WT, adaptor Δ, and *fis1-3 mdv1::HIS3* strains as WT (more than two free tubule ends in the mother cell) or fission mutant (less than three free tubule ends in the mother cell). Localization of GFP fusions GFP-Mdv1, GFP-mdv1^{CC7}, GFP-mdv1^{HR2}, GFP-mdv1$^{\Delta 2HR}$, and GFP-mdv1$^{\Delta 4HR}$ were scored in WT or adaptor Δ strains expressing mitochondrial-targeted fast-folding RFP (mito-RFP). GFP-Dnm1 localization/puncta formation was analyzed in the adaptor Δ strain containing genomically integrated *GFP-DNM1*. Overnight cultures grown at 30°C in appropriate synthetic dextrose dropout media containing 0.1 mg/ml methionine were diluted to ∼0.2 OD_{600} and grown for 3–5 h (OD_{600}, 0.5–1.0). Under these conditions, the *MET25* (methionine repressible) promoter is leaky. The abundance of proteins expressed from the uninduced *MET25* promoter was about fourfold greater than that of endogenously expressed Mdv1 (Karren et al., 2005). For analysis of dominant-negative phenotypes, cells were diluted in medium lacking methionine and grown for 4 h before scoring. The steady-state abundance of proteins expressed from the *MET25* promoter after a 4-h induction were ∼3–4-fold higher than that of uninduced Mdv1 expressed from the same promoter (Fig. S4, A and B; Karren et al., 2005). For analysis in the *fis1-3 mdv1::HIS3* strain, cells grown overnight at 25°C were diluted in medium lacking methionine and grown for 2 h at 25 or 37°C before scoring. Phenotypes were analyzed in 100 cells in three or more independent experiments. Data reported are the means of all experiments ($n \geq 3$) with the indicated standard deviations. Images were acquired and processed as described previously (Amiott et al., 2009). Cells were visualized on an imaging microscope (Axioplan 2; Carl Zeiss, Inc.) with a 100× NA 1.4 oil immersion objective. Digital fluorescence and differential interference contrast (DIC) images of cells were acquired using a monochrome digital camera (AxioCam MRm; Carl Zeiss, Inc.). Z stacks of 0.2-µm slices were obtained and deconvolved using AxioVision software (version 4.6; Carl Zeiss, Inc.). Three-dimensional projections of mitochondria were generated with the transparency (voxel) setting and converted to a single image. Final images were processed and assembled using Photoshop and Illustrator (CS3; Adobe). Brightness and contrast were adjusted using only linear operations applied to the entire image.

Analysis of protein expression and targeting

Protein expression was analyzed in WCEs prepared by the alkaline extraction method (Kushnirov, 2000). To analyze subcellular localization of proteins, cells grown in the appropriate synthetic galactose dropout medium were spheroplasted and homogenized to produce WCE, which was subsequently subjected to differential sedimentation to isolate postmitochondrial supernatant and mitochondrial pellet enriched fractions (Kondo-Okamoto et al., 2003). Either 0.5 OD_{600} equivalents of alkaline extract or 50 µg protein of WCE, 50 µg postmitochondrial supernatant, and 25 µg mitochondrial pellet fractions were separated by SDS-PAGE and analyzed by Western blotting using anti-HA (1:2,000; University of Utah Core Facility), anti-PGK (1:2,000; Invitrogen), anti-porin (1:2,000; Invitrogen), and HRP-conjugated secondary goat anti–mouse antibody (1:10,000; Sigma-Aldrich). Proteins were detected by ECL (GE Healthcare). Steady-state abundance of HA-tagged WT and mutant Mdv1 proteins (Fig. S4, A and B) expressed from the *MET25* promoter was determined in adaptor Δ cells grown for 4 h after dilution in selective medium containing 0.1 mg/ml methionine or lacking methionine. Alkali protein extracts (0.25 OD_{600} cell equivalents) separated by SDS-PAGE were analyzed by Western blotting with anti-HA primary antibody and fluorescent secondary antibody followed by detection using a scanner (Odyssey; LI-COR Biosciences). The mean intensity of each HA-tagged protein band was normalized to a control 3PGK protein band in each lane. To determine fold induction of *MET25*-regulated protein expression, normalized HA signals from induced and uninduced samples were compared. Bars in uninduced and induced graphs represent the abundance of HA-tagged signal in each lane relative to WT. Error bars indicate the standard deviation from three independent experiments.

Co-IP assays

For Mdv1–Mdv1 and Mdv1–Fis1 interaction experiments, functional HA- and Myc-tagged Mdv1 and Fis1 proteins and variants were expressed in adaptor Δ cells or adaptor Δ cells lacking *FIS1* (*fis1Δ* adaptor Δ). coIPs were performed with anti–c-Myc agarose-conjugated beads (Sigma-Aldrich) as described previously (Karren et al., 2005; Bhar et al., 2006). In brief, 30 OD_{600} cell equivalents were harvested and lysed with glass beads in 500 µl IP buffer (0.5% Triton X-100, 150 mM NaCl, 1 mM EDTA, 50 mM Tris, pH 7.4, and 1:500 protease inhibitor cocktail set III [EMD]). After centrifugation at 18,000 *g* for 10 min, 400 µl supernatant was incubated with 40 µl anti–c-Myc–conjugated agarose beads (Sigma-Aldrich) for 1 h at 4°C. Agarose beads were collected, washed in IP buffer, and incubated in 60 µl SDS-PAGE sample buffer lacking r-mercaptoethanol at 60°C for 8 min to release bound proteins. After addition of 3.2 µl r-mercaptoethanol and boiling, samples were analyzed by SDS-PAGE and Western blotting with anti-Myc (Santa Cruz Biotechnology, Inc.), and anti-HA (University of Utah Core facility) antibodies. Immunoprecipitated proteins were detected using the appropriate HRP-conjugated secondary antibodies and ECL Plus (GE Healthcare) followed by exposure to film. In Fig. 6 B, detection was accomplished using fluorescent secondary antibody (IRDye 800 anti–mouse; LI-COR Biosciences), and signals were quantified using a scanner (Odyssey) and analysis software (Odyssey version 3.0; LI-COR Biosciences).

Mdv1–Dnm1 coIPs were performed using adaptor Δ cells expressing endogenous Dnm1 and plasmid-borne HA-tagged Mdv1 variants as described previously (Karren et al., 2005). 50 OD_{600} U of cells grown at 30°C were treated with 0.2 mg/ml zymolase for 60 min at 30°C. Crosslinking was performed with 2.5 mM dithiobis(succinimidyl propionate) (DSP; Thermo Fisher Scientific) for 30 min at 30°C. DSP was quenched by addition of 50 mM glycine (also present in all subsequent buffers). After homogenization, pellets were collected by spinning at 18,000 *g* for 10 min, solubilized for 10 min at 4°C in 500 µl IP buffer (1% Triton X-100, 150 mM NaCl, 30 mM Hepes-KOH, pH 7.4, and 1:500 protease inhibitor cocktail set III), and cleared by spinning for an additional 10 min at 18,000 *g*. 400 µl cleared supernatant was incubated with 40 µl anti-HA–conjugated agarose beads (Sigma-Aldrich) for 1 h at 4°C. Agarose beads were collected, washed in IP buffer, and bound proteins were released as described in the previous paragraph. Samples were analyzed by SDS-PAGE and ECL Western blotting with anti-HA and anti-Dnm1 antibodies (Otsuga et al., 1998).

Online supplemental material

Fig. S1 shows additional analysis of mdv1^{HR2} localization and function. Fig. S2 shows that Glu250 is exposed on one face of the dimeric antiparallel CC. Fig. S3 shows an additional analysis of mdv1^{D2HR} and mdv1^{D4HR} proteins. Fig. S4 shows dominant-negative effects of WT and mutant Mdv1 proteins. Table S1 shows plasmids used in this study. Table S2 shows x-ray data and model statistics. Online supplemental material is available at http://www.jcb.org/cgi/content/full/jcb.201005046/DC1.

We thank Jane Macfarlane for expertise in mutagenesis and plasmid construction, Steve Alam for advice regarding protein purification, and members of the Shaw laboratory for critical discussions.

Research support was provided by the National Institutes of Health (grants GM53466 to J.M. Shaw, GM59135 to C.P. Hill, and GM82545 to M.S. Kay). Support for sequencing, antibody, and oligonucleotide services at the University of Utah is provided by the National Institutes of Health Center for Cancer Research Resources (grant M01RR00064). Portions of this research were carried out at the Stanford Synchrotron Radiation Light Source (SSRL) Office of Basic Energy Sciences, a national user facility operated by Stanford University on behalf of the U.S. Department of Energy. The SSRL Structural Molecular Biology Program is supported by the Department of Energy, the Office of Biological and Environmental Research, and the National Institutes of Health, National Center for Research Resources, Biomedical Technology Program, and National Institute of General Medical Sciences.

Submitted: 11 May 2010
Accepted: 8 November 2010

References

Amiott, E.A., M.M. Cohen, Y. Saint-Georges, A.M. Weissman, and J.M. Shaw. 2009. A mutation associated with CMT2A neuropathy causes defects in Fzo1 GTP hydrolysis, ubiquitylation, and protein turnover. *Mol. Biol. Cell.* 20:5026–5035. doi:10.1091/mbc.E09-07-0622

Bhar, D., M.A. Karren, M. Babst, and J.M. Shaw. 2006. Dimeric Dnm1-G385D interacts with Mdv1 on mitochondria and can be stimulated to assemble into fission complexes containing Mdv1 and Fis1. *J. Biol. Chem.* 281:17312–17320. doi:10.1074/jbc.M513530200

Bleazard, W., J.M. McCaffery, E.J. King, S. Bale, A. Mozdy, Q. Tieu, J. Nunnari, and J.M. Shaw. 1999. The dynamin-related GTPase Dnm1 regulates mitochondrial fission in yeast. *Nat. Cell Biol.* 1:298–304. doi:10.1038/13014

Collaborative Computational Project 4. 1994. The CCP4 suite: programs for protein crystallography. *Acta Crystallogr. D. Biol. Crystallogr.* D50:760–763.

Cerveny, K.L., and R.E. Jensen. 2003. The WD-repeats of Net2p interact with Dnm1p and Fis1p to regulate division of mitochondria. *Mol. Biol. Cell.* 14:4126–4139. doi:10.1091/mbc.E03-02-0092

Cerveny, K.L., J.M. McCaffery, and R.E. Jensen. 2001. Division of mitochondria requires a novel DMN1-interacting protein, Net2p. *Mol. Biol. Cell.* 12:309–321.

Chen, H., and D.C. Chan. 2005. Emerging functions of mammalian mitochondrial fusion and fission. *Hum. Mol. Genet.* 2:R283–R289. doi:10.1093/hmg/ddi270

Cole, J.L. 2004. Analysis of heterogeneous interactions. *Methods Enzymol.* 384:212–232. doi:10.1016/S0076-6879(04)84013-8

Emsley, P., and K. Cowtan. 2004. Coot: model-building tools for molecular graphics. *Acta Crystallogr. D Biol. Crystallogr.* 60:2126–2132. doi:10.1107/S0907444904019158

Griffin, E.E., J. Graumann, and D.C. Chan. 2005. The WD40 protein Caf4p is a component of the mitochondrial fission machinery and recruits Dnm1p to mitochondria. *J. Cell Biol.* 170:237–248. doi:10.1083/jcb.200503148

Ingerman, E., E.M. Perkins, M. Marino, J.A. Mears, J.M. McCaffery, J.E. Hinshaw, and J. Nunnari. 2005. Dnm1 forms spirals that are structurally tailored to fit mitochondria. *J. Cell Biol.* 170:1021–1027. doi:10.1083/jcb.200506078

Karren, M.A., E.M. Coonrod, T.K. Anderson, and J.M. Shaw. 2005. The role of Fis1p-Mdv1p interactions in mitochondrial fission complex assembly. *J. Cell Biol.* 171:291–301. doi:10.1083/jcb.200506158

Kondo-Okamoto, N., J.M. Shaw, and K. Okamoto. 2003. Mmm1p spans both the outer and inner mitochondrial membranes and contains distinct domains for targeting and foci formation. *J. Biol. Chem.* 278:48997–49005. doi:10.1074/jbc.M308436200

Koshiba, T., S.A. Detmer, J.T. Kaiser, H. Chen, J.M. McCaffery, and D.C. Chan. 2004. Structural basis of mitochondrial tethering by mitofusin complexes. *Science.* 305:858–862. doi:10.1126/science.1099793

Kushnirov, V.V. 2000. Rapid and reliable protein extraction from yeast. *Yeast.* 16:857–860. doi:10.1002/1097-0061(20000630)16:9<857::AID-YEA561>3.0.CO;2-B

Lackner, L.L., J.S. Horner, and J. Nunnari. 2009. Mechanistic analysis of a dynamin effector. *Science.* 325:874–877. doi:10.1126/science.1176921

Laue, T., B. Shah, T. Ridgeway, and S. Pelletier. 1992. Computer-aided interpretation of analytical sedimentation data for proteins. *In* Analytical Ultracentrifugation in Biochemistry and Polymer Science. Royal Society of Chemistry, Cambridge, England, UK. 90–125.

Mozdy, A.D., J.M. McCaffery, and J.M. Shaw. 2000. Dnm1p GTPase-mediated mitochondrial fission is a multi-step process requiring the novel integral membrane component Fis1p. *J. Cell Biol.* 151:367–380. doi:10.1083/jcb.151.2.367

Murshudov, G.N., A.A. Vagin, and E.J. Dodson. 1997. Refinement of macromolecular structures by the maximum-likelihood method. *Acta Crystallogr. D Biol. Crystallogr.* 53:240–255. doi:10.1107/S0907444996012255

Naylor, K., E. Ingerman, V. Okreglak, M. Marino, J.E. Hinshaw, and J. Nunnari. 2006. Mdv1 interacts with assembled dnm1 to promote mitochondrial division. *J. Biol. Chem.* 281:2177–2183. doi:10.1074/jbc.M507943200

Okamoto, K., and J.M. Shaw. 2005. Mitochondrial morphology and dynamics in yeast and multicellular eukaryotes. *Annu. Rev. Genet.* 39:503–536. doi:10.1146/annurev.genet.38.072902.093019

Otsuga, D., B.R. Keegan, E. Brisch, J.W. Thatcher, G.J. Hermann, W. Bleazard, and J.M. Shaw. 1998. The dynamin-related GTPase, Dnm1p, controls mitochondrial morphology in yeast. *J. Cell Biol.* 143:333–349. doi:10.1083/jcb.143.2.333

Otwinowski, Z., and W. Minor. 1997. Processing of x-ray diffraction data collected in oscillation mode. *In* Methods in Enzymology. Macromolecular Crystallography, part A. Vol. 276. C.W. Carter, Jr. and R.M. Sweet, editors. Academic Press, New York. 307–326.

Shaw, J.M., and J. Nunnari. 2002. Mitochondrial dynamics and division in budding yeast. *Trends Cell Biol.* 12:178–184. doi:10.1016/S0962-8924(01)02246-2

Studier, F.W. 2005. Protein production by auto-induction in high density shaking cultures. *Protein Expr. Purif.* 41:207–234. doi:10.1016/j.pep.2005.01.016

Suzuki, M., A. Neutzner, N. Tjandra, and R.J. Youle. 2005. Novel structure of the N terminus in yeast Fis1 correlates with a specialized function in mitochondrial fission. *J. Biol. Chem.* 280:21444–21452. doi:10.1074/jbc.M414092200

Terwilliger, T.C., and J. Berendzen. 1999. Automated MAD and MIR structure solution. *Acta Crystallogr. D Biol. Crystallogr.* 55:849–861. doi:10.1107/S0907444999000839

Tieu, Q., and J. Nunnari. 2000. Mdv1p is a WD repeat protein that interacts with the dynamin-related GTPase, Dnm1p, to trigger mitochondrial division. *J. Cell Biol.* 151:353–366. doi:10.1083/jcb.151.2.353

Tieu, Q., V. Okreglak, K. Naylor, and J. Nunnari. 2002. The WD repeat protein, Mdv1p, functions as a molecular adaptor by interacting with Dnm1p and Fis1p during mitochondrial fission. *J. Cell Biol.* 158:445–452. doi:10.1083/jcb.200205031

Wolf, E., P.S. Kim, and B. Berger. 1997. MultiCoil: a program for predicting two- and three-stranded coiled coils. *Protein Sci.* 6:1179–1189. doi:10.1002/pro.5560060606

Zhang, Y., and D.C. Chan. 2007. Structural basis for recruitment of mitochondrial fission complexes by Fis1. *Proc. Natl. Acad. Sci. USA.* 104:18526–18530. doi:10.1073/pnas.0706441104

Published December 13, 2010

Koirala et al., http://www.jcb.org/cgi/content/full/jcb.201005046/DC1

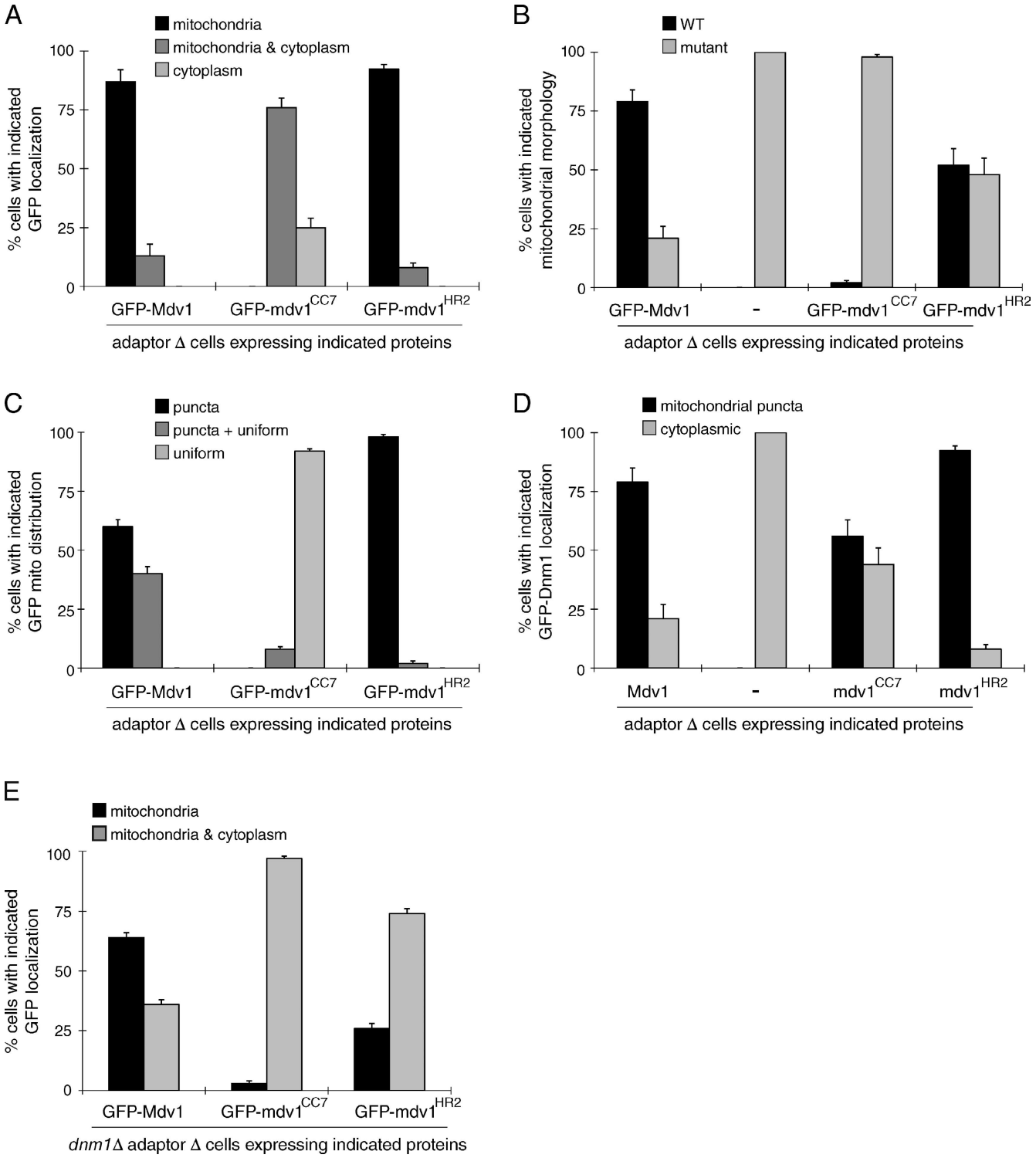

Figure S1. **Additional Analysis of mdv1^{HR2} localization and function.** (A) Subcellular localization of N-terminal GFP-tagged Mdv1, mdv1^{CC7}, and mdv1^{HR2} proteins in adaptor Δ cells. (B) Mitochondrial morphologies in adaptor Δ cells expressing GFP-tagged Mdv1, mdv1^{CC7}, and mdv1^{HR2} proteins. (C) Mitochondrial distribution of GFP-tagged Mdv1, mdv1^{CC7}, and mdv1^{HR2} proteins. (D) Localization of genomically expressed GFP-Dnm1 in cells expressing Mdv1, mdv1^{CC7}, or mdv1^{HR2}. (E) Subcellular localization of GFP-tagged Mdv1, mdv1^{CC7}, and mdv1^{HR2} proteins in *dnm1*Δ adaptor Δ cells. Error bars represent the mean and standard deviation of at least three independent experiments (n = 100).

Published December 13, 2010

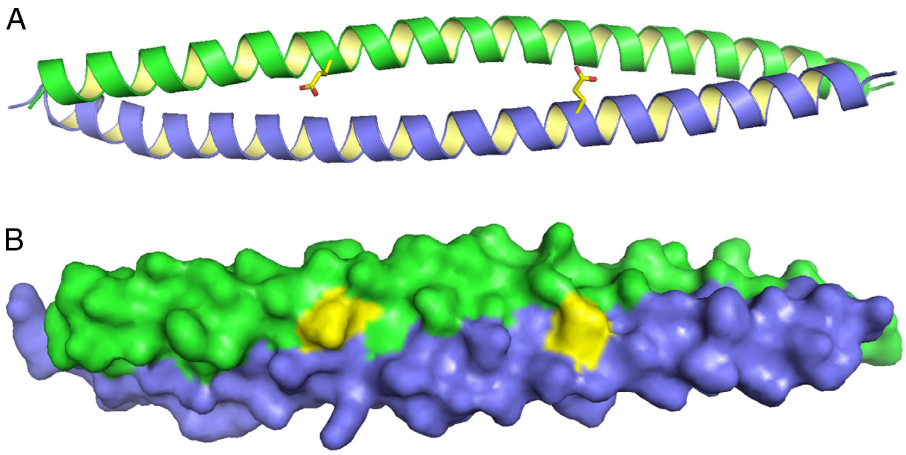

Figure S2. **Glu250 is exposed on one face of the dimeric antiparallel CC.** (A and B) Positions of E250 residues on the Mdv1 CC structure are shown as yellow side chains on the ribbon structure (A) and as yellow patches on the space-filling model (B). The different α-helices in the CC are shown in green and blue.

Published December 13, 2010

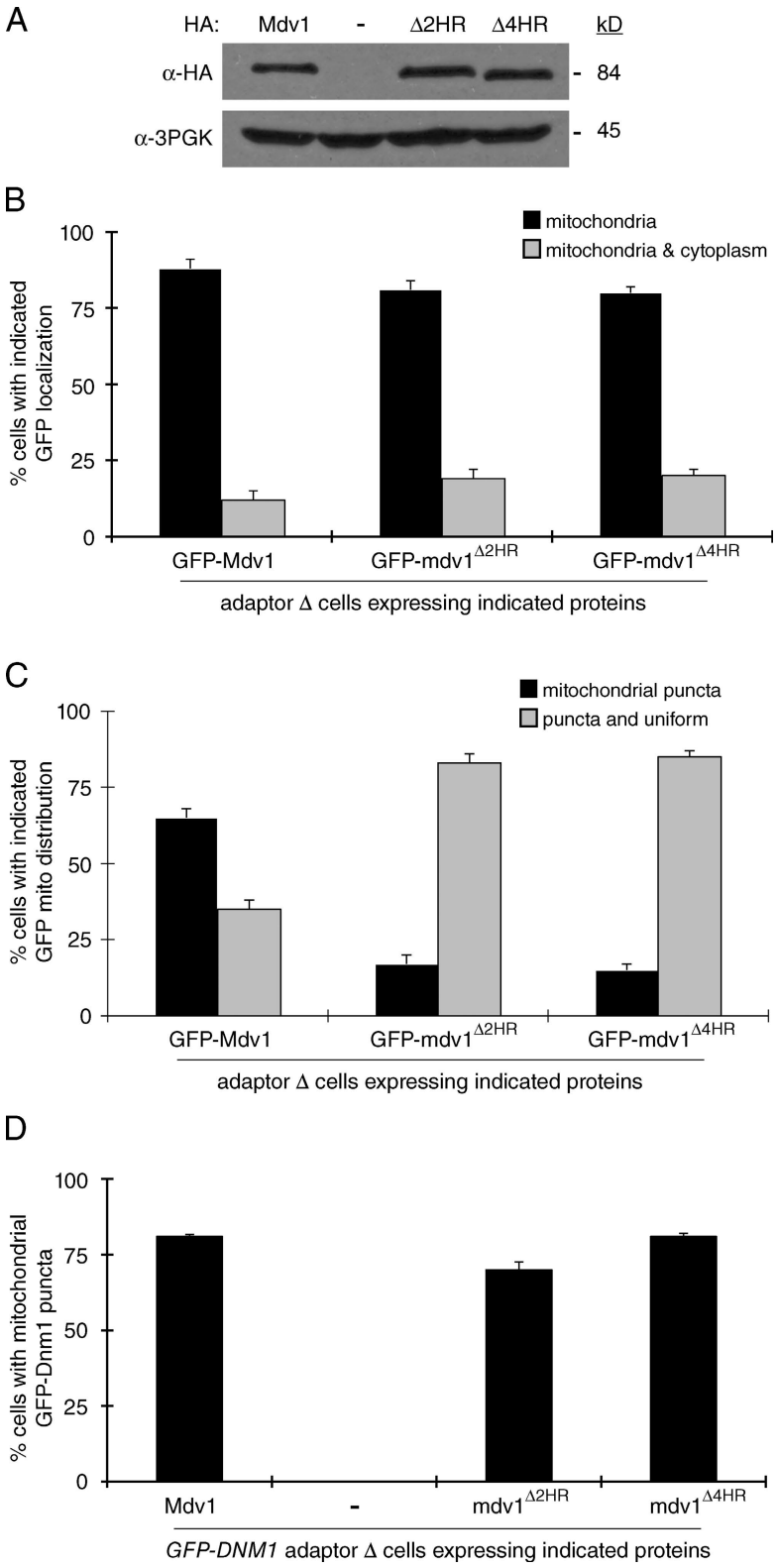

Figure S3. **Additional analysis of mdv1$^{\Delta 2HR}$ and mdv1$^{\Delta 4HR}$ proteins.** (A) Steady-state abundance of C-terminal HA-tagged Mdv1, mdv1$^{\Delta 2HR}$, and mdv1$^{\Delta 4HR}$ proteins expressed in adaptor Δ cells. WCEs separated by SDS-PAGE were immunoblotted with anti-HA and anti-3PGK antibodies. (B) Mitochondrial distribution of GFP-tagged WT and ΔHR mutant Mdv1 proteins. (C) Mitochondrial distribution of GFP-tagged Mdv1, mdv1$^{\Delta 2HR}$, and mdv1$^{\Delta 4HR}$ proteins imaged in adaptor Δ cells. (D) Localization of genomically expressed GFP-Dnm1 in cells expressing Mdv1, mdv1$^{\Delta 2HR}$, and mdv1$^{\Delta 4HR}$ proteins. Error bars represent the mean and standard deviation of at least three independent experiments (n = 100).

Published December 13, 2010

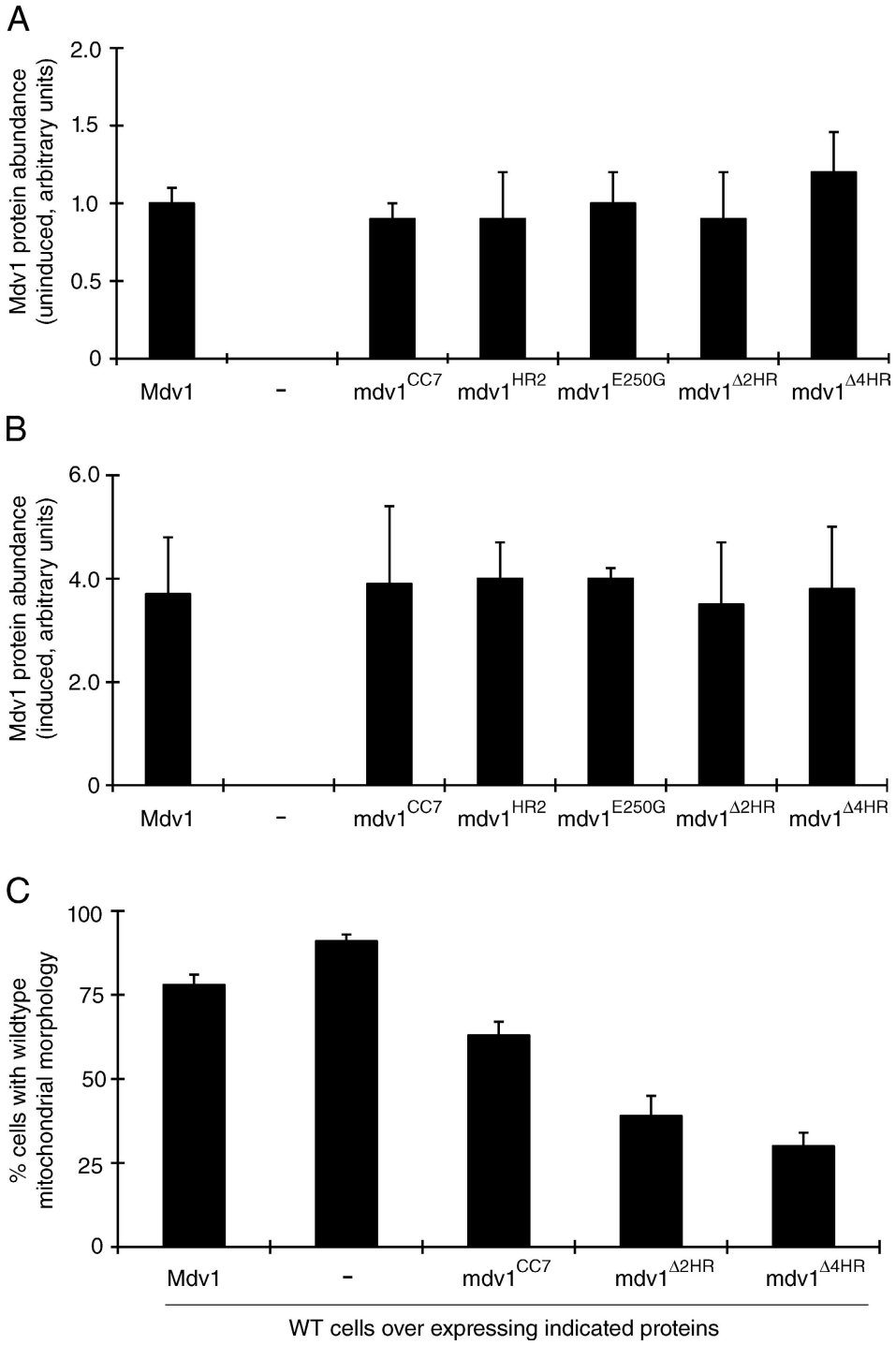

Figure S4. **Dominant-negative effects of WT and mutant Mdv1 proteins.** (A) Relative steady-state abundance of WT and mutant Mdv1 proteins expressed from the uninduced *MET25* promoter in adaptor Δ cells. (B) Relative steady-state abundance of WT and mutant proteins expressed from the induced *MET25* promoter in adaptor Δ cells. Quantification details for A and B are discussed in Materials and methods. (C) Mitochondrial morphology in WT cells expressing WT and mutant Mdv1 proteins from the *MET25* promoter after a 4-h induction. Error bars represent the mean and standard deviation of at least three independent experiments (n = 100).

Published December 13, 2010

Table S1. **Plasmids used in this study**

ID number	Plasmid	Protein expressed	Source
B493	*pRS415MET25*	None	ATCC 87322
B494	*pRS416MET25*	None	ATCC 87324
B824	*pRS415MET25-9MYC-FIS1*	9Myc-Fis1	Karren et al., 2005
B1642	*p414GPD-mt-ffRFP*	*N. crassa* ATP9(1–69) + fast-folding DsRed	Karren et al., 2005
B1808	*pRS415MET25-MDV1*	MDV1	Karren et al., 2005
B2053	*pRS416MET25-MDV1*	MDV1	Karren et al., 2005
B2054	*pRS416MET25-mdv1^{E250G}*	Mdv1^{E250G}	Karren et al., 2005
B2499	*pMAL-c2x-mdv1-CC*	10xHIS-PPCS-mdv1-CC	This study
B2620	*pRS416MET25-mdv1^{CC7}*	mdv1$^{L233E,\ L237E,\ I251E,\ I254E,\ L268E,\ I272E,\ I275E}$	This study
B2621	*pMAL-c2x-mdv1-CC^{SeMet}*	mdv1-CC$^{L248M,\ L281M}$	This study
B2683	*pRS415MET25-GFP-mdv1^{CC7}*	GFP-mdv1^{CC7}	This study
B2783	*pRS416MET25-mdv1^{HR2}*	Mdv1$^{1–229}$–*M. musculus* Mfn1$^{674–734}$–Mdv1$^{295–714}$	This study
B2798	*pRS416MET25-mdv1^{CC7}-13MYC*	mdv1^{CC7}-13MYC	This study
B2800	*pRS415MET25-mdv1^{HR2}-13MYC*	mdv1^{HR2}-13MYC	This study
B2821	*pRS415MET25-MDV1-3HA*	Mdv1-3HA	This study
B2832	*pRS416MET25-mdv1^{HR2}-3HA*	mdv1^{HR2}-3HA	This study
B2833	*pRS416MET25-mdv1^{HR2}-13MYC*	mdv1^{HR2}-13MYC	This study
B2837	*pRS416MET25-MDV1-13MYC*	Mdv1-13MYC	This study
B2839	*pRS415MET25-mdv1^{CC7}-3HA*	mdv1^{CC7}-3HA	This study
B2864	*pRS416MET25-9MYC-FIS1*	9MYC-Fis1	This study
B2882	*pRS415MET25-mdv1^{E250G}-3HA*	mdv1^{E250G}-3HA	This study
B2892	*pRS415MET25-GFP-mdv1^{HR2}*	GFP-mdv1^{HR2}	This study
B3003	*pRS416MET25-ffRFP-mdv1^{CC7}*	ffRFP-mdv1^{CC7}	This study
B3015	*pRS416MET25-mdv1$^{\Delta 2HR}$*	mdv1$^{\Delta 2HR}$	This study
B3016	*pRS416MET25-mdv1$^{\Delta 4HR}$*	mdv1$^{\Delta 4HR}$	This study
B3017	*pRS415MET25-mdv1$^{\Delta 2HR}$-3HA*	mdv1$^{\Delta 2HR}$-3HA	This study
B3018	*pRS415MET25-mdv1$^{\Delta 4HR}$-3HA*	mdv1$^{\Delta 4HR}$-3HA	This study
B3028	*pRS415MET25-GFP-mdv1$^{\Delta 2HR}$*	GFP-mdv1$^{\Delta 2HR}$	This study
B3029	*pRS415MET25-GFP-mdv1$^{\Delta 4HR}$*	GFP-mdv1$^{\Delta 4HR}$	This study

ATCC, American Type Culture Collection.

Table S2. **X-ray data and model statistics**

Space group $P4_12_12$	*SeMdv13* Se peak	*SeMdv13* Se inflection
Data collection		
Cell a =, c = (Å)	41.38, 227.38	41.35, 227.39
Resolution (Å)	38–2.7	38–2.8
(high)	(2.79–2.7)	(2.9–2.8)
No. unique reflections	10,392	9,222
Rmerge	5.3 (27.9)	6.4 (21.1)
Completeness	99.2 (99.2)	98.8 (98.5)
I–SigI	10.0 (2.4)	10.2 (2.31)
Redundancy	1.8 (1.7)	1.8 (1.7)
Refinement		
R/Rfree	27.0/31.4	NA
No. protein atoms	1,067	NA
No. water atoms	21	NA
<B> protein	58.5	NA
<B> water	52.1	NA
Rms bond (Å)	0.014	NA
Rms angle (°)	1.5	NA

NA, not applicable.

Published December 13, 2010

Reference

Karren, M.A., E.M. Coonrod, T.K. Anderson, and J.M. Shaw. 2005. The role of Fis1p–Mdv1p interactions in mitochondrial fission complex assembly. *J. Cell Biol.* 171:291–301. doi:10.1083/jcb.200506158